1-1-2003

Investigations of Supramolecular and Catalytic Properties of PPI Dendrimers

Aaron K. Holley
aaron.holley@uky.edu

Investigations of Supramolecular and Catalytic Properties of PPI Dendrimers

Thesis submitted to
The Graduate College of
Marshall University

In partial fulfillment of the
Requirements for the degree of
Master of Science
Chemistry

by

Aaron K. Holley

Marshall University

09 July 2003

This thesis was accepted on _____
Month Day Year

as meeting the research requirements for the master's degree.

Advisor_____

Department of _____

_____
Dean of the Graduate College

Abstract

INVESTIGATIONS OF SUPRAMOLECULAR AND CATALYTIC PROPERTIES OF PPI DENDRIMERS

by Aaron K. Holley

The research reported in this thesis focused on supramolecular and catalytic properties of **p**oly(**p**ropylene **i**mine) (PPI) dendrimers. Analytical techniques used in this research included high resolution NMR spectroscopy, as well as UV-vis and fluorescence spectroscopies and scanning electron microscopy. This investigation showed that: (1) PPI dendrimers interact with diacids to form interlock self-assemblies by electrostatic interactions (with an increase in dendrimer generation, smaller diacids are required to form the most efficient self-assembly); (2) PPI/diacid self-assemblies are able to encapsulate fluorescent dyes within the void spaces of the PPI/diacid moieties; (3) PPI-3 can chelate many types of metal cations, and these cations compete for the binding sites along the surface of the dendrimer; (4) PPI-3 can catalyze the hydrolysis of esters under very mild conditions (mildly basic pH and room temperature).

DEDICATION

To my parents and my sister for their love and support throughout the course of this study and throughout my life.

ACKNOWLEDGEMENTS

I wish to express my sincere gratitude and thanks to my graduate research advisor, Dr. Minghui Chai, for her dedication and for her advice on this research and throughout the entire course of my graduate studies at Marshall University. I would also like to thank Drs. Robert Morgan and Michael Norton for their collaboration on this research, and Mr. David Neff for his instruction and assistance on operation of the SEM. I also wish to acknowledge the rest of the faculty and the staff of the Chemistry department.

I wish to acknowledge the Marshall University Science Faculty NASA Research Enhancement Award(s) (REA) and Marshall University Pilot Research Award for financial support of this research, as well as NSF-WV EPSCOR for the purchase of the 500 MHz NMR spectrometer used in this study.

TABLE OF CONTENTS

LIST OF FIGURES

LIST OF TABLES

LIST OF SYMBOLS AND NOMENCLATURE

$DABF_4$.....dipyrido[1,2-c:2',1'-e] imidazol-5-ium, 6(dimethylamine)-2,10-bis (hydroxycarbonyl), tetrafluoroborate

$DEBF_4$..... dipyrido[1,2-c:2',1'-e] imidazol-5-ium, 6(dimethylamine)-2,10-bis (methoxycarbonyl), tetrafluoroborate

λ_{max}..... .....maximum wavelength

HETCOR..... .....**Het**eronuclear **Cor**relation

NMR.....**N**uclear **M**agnetic **R**esonance

NOESY.....**N**uclear **O**verhauser **E**ffect **S**pectroscop**y**

PPI.....**p**oly(**p**ropylene **i**mine)

PAMAM.....**p**oly(**a**mido**a**mine)

UV-vis.....**U**ltra**v**iolet-**v**isible

SEM.....**S**canning **E**lectron **M**icroscopy

TOCSY.....**To**tal **C**orrelation **S**pectroscop**y**

T_1..... .....spin-lattice relaxation

Chapter 1: Brief Introduction to Dendrimers

Dendrimers are an interesting class of macromolecules that have a highly symmetrical, hyper-branched and spherical structure. Dendrimers possess an architecture consisting of: (1) a core; (2) an interior of shells (generation); and (3) an exterior (outermost layer), which often has terminal functional groups (Figure 1.1).[1] The core determines the size and shape of the dendrimer, the interior determines the amount of void space that can be enclosed by the dendrimer, and the exterior allows growth of the dendrimer or other chemical modification. This unique architecture makes dendrimers monodisperse macromolecules compared to classical linear polymers. In dendritic structures, the number of terminal groups increase exponentially with a linear increase in the generation of the dendrimer. This relationship limits the ultimate size of the dendrimer due to steric crowding of the terminal groups.[2]

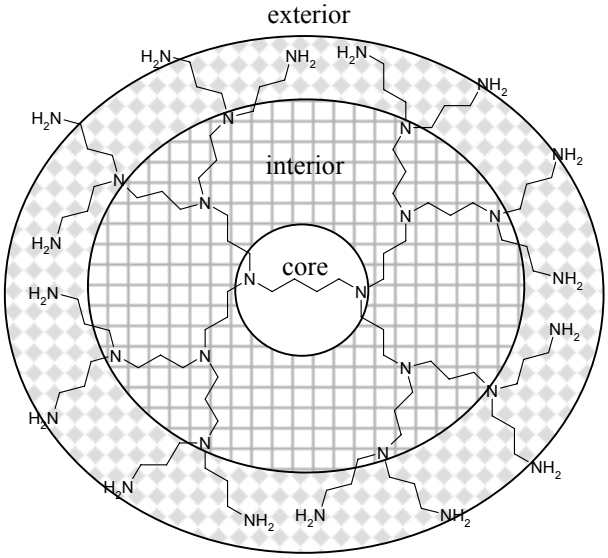

Figure 1.1. Structural components of a dendrimer.

The first synthesis of a dendrimer was reported by Vögtle *et al*, in which acrylonitrile was added to an amine by a double Michael addition followed by reduction using the homogeneous reducing agent Co(II) with $NaBH_4$.[3] However, large-scale synthesis using this method was difficult due to the coordination of the final products with metal cations, which caused problems in separation and purification of the final products. Fifteen years later, large-scale synthesis of dendrimers was reported by Wörner and Mülhaupt[4] using an ammonia core and acrylonitrile monomers, and by de Brabander-van den Berg and Meijer[5] using a diaminobutane core with acrylonitrile monomers (PPI dendrimer). Both groups used a modified Vögtle procedure employing a heterogeneous catalyst of Raney Co and H_2 to reduce the cyano groups to amines (Figure 1.2). Large quantities of PPI dendrimer are commercially available from Aldrich Chemical Company, and DSM, the Netherlands. PPI is available in a variety of generations, with generation 5 being the largest dendrimer (Figure 1.3).

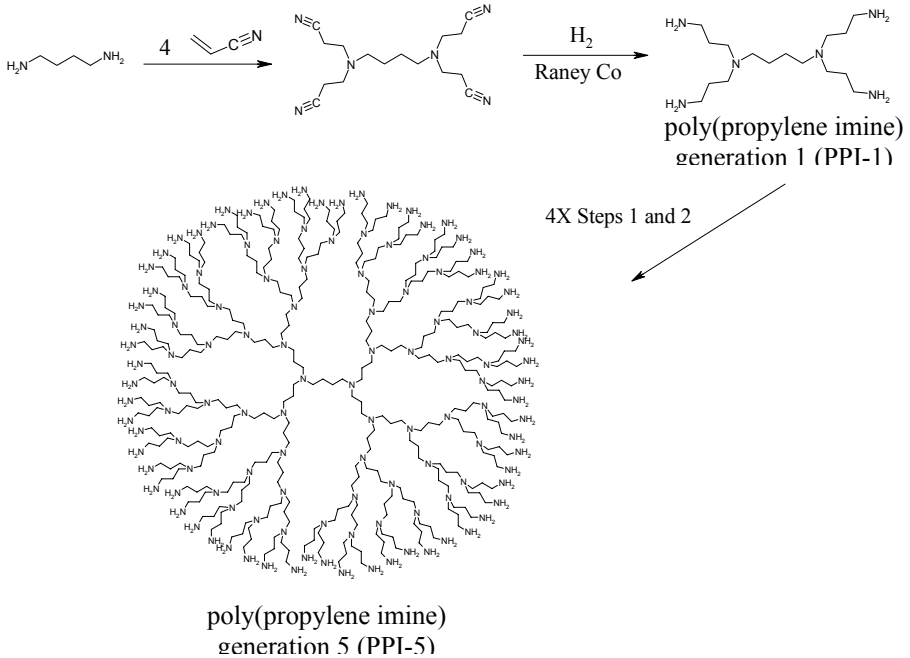

Figure 1.2. Scheme for the divergent method of dendrimer synthesis.

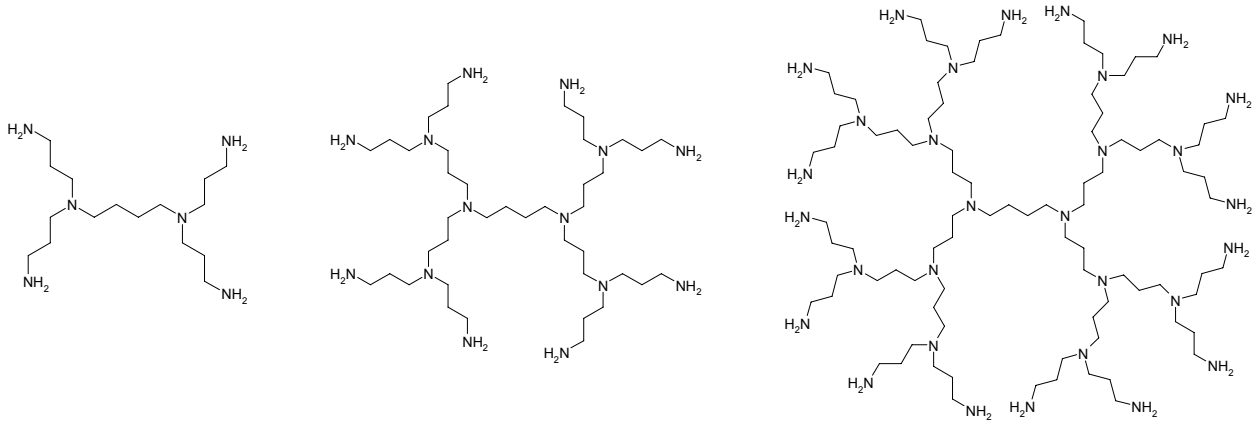

PPI-1 **PPI-2** **PPI-3**

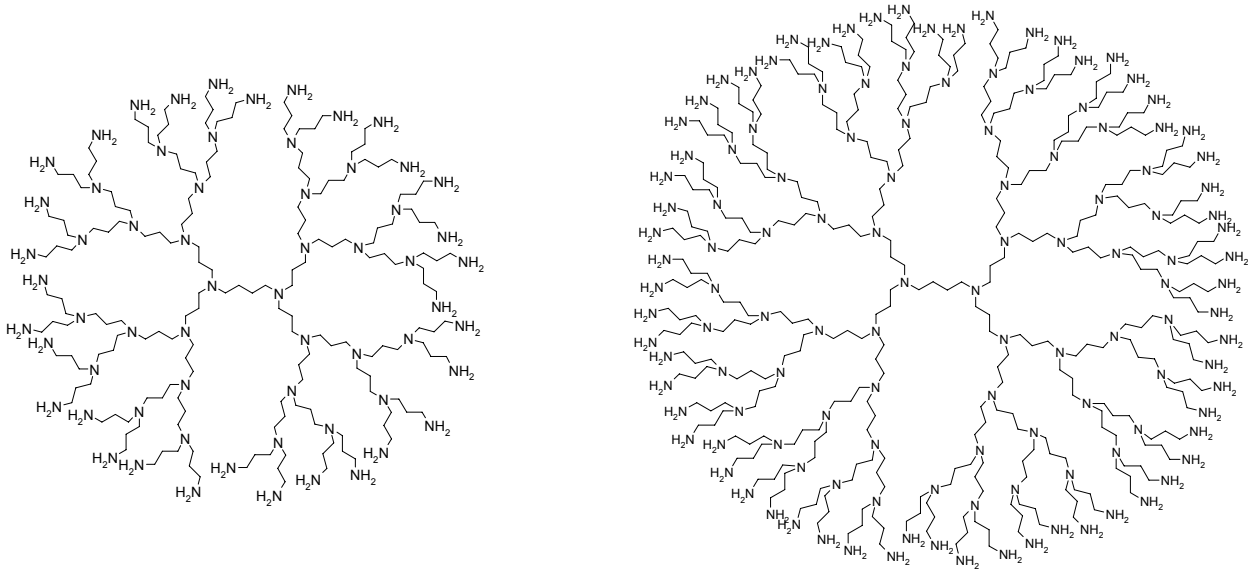

PPI-4 **PPI-5**

Figure 1.3. Different generations of the PPI dendrimer.

Two synthetic routes exist for the synthesis of dendrimers: the divergent method and the convergent method. In the divergent method, the monomer units are added to a multifunctional core to form early, low molecular weight generations of the dendrimer. Successive groups of monomers are added to form higher generations of the dendrimer

(Figure 1.2).[3,4,5] This method can best be thought of as an "inside-out" method of producing dendrimers.

In the convergent method, dendrimers are built from the outside toward the core. Synthesis starts with monomers that will become the exterior. These monomers are attached to an "anchor" to form dendritic wedges (or dendrons). The resulting dendritic wedges are eventually added to a multifunctional core molecule, resulting in a full dendrimer (Figure 1.4).[6,7] The convergent method has certain advantages over the divergent method: (1) small number of coupling reactions per generation resulting in greater control over synthesis; (2) a minimization of reaction failure; and (3) simplified purification procedure.[7]

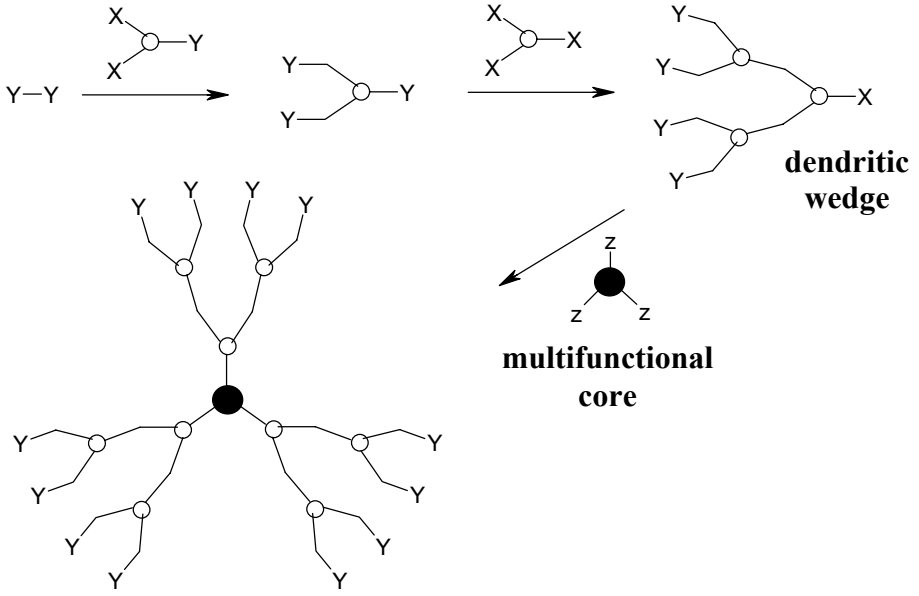

Figure 1.4. Scheme for convergent method of dendrimer synthesis.

The distinct structure of dendrimers gives them many unique physical and chemical properties compared to their linear polymer analogs. Linear polymers show an increase in intrinsic viscosity with an increase in molecular weight. Dendrimers have a

much lower intrinsic viscosity and do not show this trend with increasing molecular weight. Dendrimers also have a much higher solubility than linear polymers with similar molecular weight, type of monomers, and number of functional groups. These properties can be explained by the globular shape and high number of functional groups of dendrimers. These structural components enhance interactions between the dendrimer and their environment.[8]

The presence internal void spaces (a.k.a. dendritic voids), a uniform size and spherical shape, and a multifunctional periphery makes dendrimers specially suitable for various applications in many areas.[9] The void spaces within dendrimers makes them useful for the encapsulation of a variety of small guest molecules such as dyes for fluorescent markers,[10] and drug molecules for drug delivery.[11] An advantage of using dendrimers as drug delivery agents is their ability to circulate through the body for long periods, as well as protect the drug molecules from inactivation by shielding them from the body's environment. A dendrimer with a hydrophobic interior and hydrophilic exterior as a dendritic unimolecular micelle was shown to encapsulate the drug indomethacin. Studies of the drug release characteristics *in vitro* showed that the drug was released much more slowly when encapsulated than when unencapsulated.[11]

The peripheral functional groups allows modification of the surface of the dendrimer.[12] This ease in modification can be exploited to tailor the properties of the dendrimer for specific applications. In one study, a series of dendrimers based on 3,3'-iminobis(propylamine) core with *N*-acetylneuraminic acid (sialic acid) units on the surface were synthesized. These dendrimers were found to directly bind the sialic acid specific animal lectin *Limax flavus* (LFA) and to inhibit the binding of this lectin to

human α-acid glycoprotein, showing that these dendrimers have potential applications in drug targeting.[13]

Dendrimers also have a wide variety of industrial applications. Dendrimers can act as catalysts or reaction vessels for chemical reactions. Catalytic sites on the dendrimer can be metallic or non-metallic in nature,[14,15] and can be located at the core, within the interior, or at the periphery of the dendrimer.[16] These unique features of dendrimers makes them promising materials that may have a dramatic impact on our everyday lives.

Chapter 2: NMR Studies of Self-Assemblies of PPI Dendrimers and Diacid Acids

Introduction

The spontaneous self-assembly of molecules to form supramolecular arrays through non-covalent interactions (hydrogen bonding, electrostatic interaction, and hydrophobic interaction, etc.) plays an important role in the function and three-dimensional structure of many biologically important molecules, such as DNA and proteins.[17] Self-assembly has become a unique and useful way for researchers to synthesize artificial nanoscopic structures that would not be possible through standard synthetic routes.[18]

In one study, well-defined aggregates were formed by adding stoichiometric amounts of calix[4]arene dimelamines with 5,5-diethylbarbituric acids (DEB). These aggregates were held together by 72 hydrogen bonds.[19] Later, the same group of researchers were able to synthesize hydrogen-bonded polymeric nanorods using calix[4]arene dimelamine with calix[4]arene dicyanurate.[20] Whitesides *et al* synthesized supramolecular rosettes through the self-assembly of melamine and cyanuric acid.[21]

Dendrimers make ideal scaffolds for self-assemblies because of their nanoscopic sizes and unique structures.[22] The multifunctional surface of dendrimers can be readily modified by reacting with a variety of molecules, which can tune the self-assembly properties of dendrimers. Meijer *et al* modified the periphery of PPI dendrimers into adamantylurea end groups and then added glycinylurea derivatives to form self-assemblies through a combination of electrostatic interactions and hydrogen bonds.[23]

Unmodified dendrimers have also been reported as scaffolds for self-assemblies. Crooks *et al* used electrostatic interactions to form self-assembled inverse micelles between PAMAM dendrimers and long-chain monoacids.[24] These self-assemblies were formed based on acid-base reactions between the peripheral amines of the dendrimer and the carboxylic acid groups of the acids to form ion pairs. In this study, the formation of these ion pairs was reversible, which can be controlled by changing the pH of the system. These inverse micelles can be used to encapsulate polar guest molecules and to shuttle these molecules between hydrophilic and hydrophobic phases based on the pH-sensitivity of the self-assembly.

Up to now, much work has been reported using monoacids to form self-assemblies based on dendrimer templates.[24] However, little work has been reported using dendrimers and diacids. Ideal intramolecular self-assembly between dendrimers and diacids can possibly generate interlock structures by electrostatic interactions (Figure 2.1). Such interlocked self-assembled structures can be used to "lock" guest molecules inside dendrimer moieties for better encapsulation. In this study, a series of samples were made using different generations of PPI dendrimer (Figure 1.3) and different diacids (Figure 2.2). These samples were studied using a variety of NMR techniques to determine relationships between dendrimers and diacid acids in self-assembly.

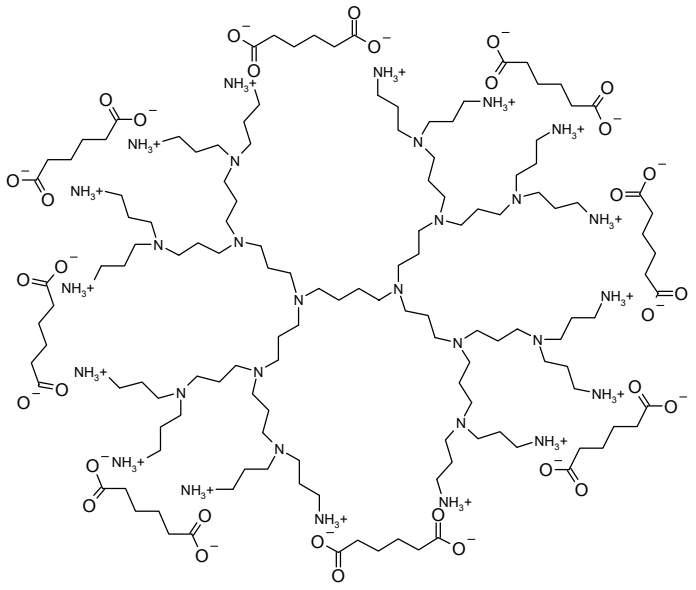

Figure 2.1. Interlock structure of PPI-3/adipic acid self-assembly.

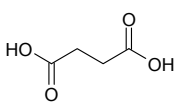

succinic acid

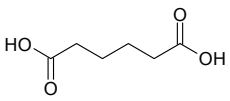

adipic acid

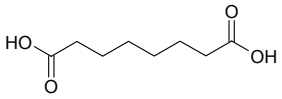

suberic acid

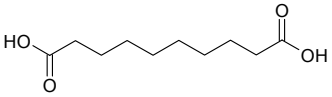

sebacic acid

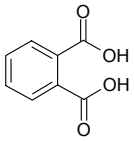

phthalic acid

Figure 2.2. The structures of diacid acids used for this study.

Experimental

Different generations of PPI dendrimers were purchased from Aldrich Chemical Co. Sebacic and adipic acids were obtained from Lancaster Synthesis, suberic acid from Sigma-Aldrich, and succinic and phthalic acids from Fisher Scientific, Inc. Deuterium oxide was purchased from Norrell, Inc. All materials were used as received without further purification.

A series of NMR samples were prepared using different generations of dendrimers mixed with stoichiometric amounts of different diacids (4:1 diacid-to-PPI-2, 8:1 diacid-to-PPI-3, 16:1 diacid-to-PPI-4), respectively, in 0.7 mL D_2O in 5 mm NMR tubes. Concentrations of all reagents are summarized in Table 2.1.

Table 2-1. Concentrations of Dendrimers and Diacids Used For This Study.

Sample	Concentration of Reagents (M)	
	Dendrimer	Diacid
PPI-2 alone	0.0216	----------
+succinic	0.0187	0.0774
+adipic	0.0194	0.0772
+suberic	0.0192	0.0746
+sebacic	0.019	0.0749
+phthalic	0.0192	0.0783
PPI-3 alone	0.0185	----------
+succinic	0.0188	0.1512
+adipic	0.0187	0.1496
+suberic	0.0188	0.1493
+sebacic	0.0187	0.1497
+phthalic	0.0191	0.1522
PPI-4 alone	0.0186	----------
+succinic	0.0185	0.2976
+adipic	0.0185	0.2962
+suberic	0.0185	0.3042
+sebacic	0.0186	0.3002
+phthalic	0.0186	0.2992

NMR spectra were collected on a Varian UnityPlus 500 MHz NMR spectrometer equipped with a Nalorac PFG triple resonance $^{1}H/^{13}C/X$ probe (X tunable from ^{15}N to ^{31}P) and a Varian broadband probe. All NMR data were processed using Varian VNMR software on a SUN UltraSPARC-60 workstation.

All ^{1}H spectra were acquired at 499.219 MHz using a 4706.4 Hz spectral window, 5.5 μs (60^{o}) pulse width, and 64 transients. 2D ^{1}H-^{1}H TOCSY NMR spectra were obtained at 499.220 MHz using a 2499.5 Hz spectral window, 7.5-8.5 μs (90^{o}) pulse width, with a 1 s relaxation delay, a 0.256 s acquisition time, and 8 transients. Data

processing was performed with Gaussian weighting in both dimensions and zero filling to display the data on a 2560x1024 two-dimensional matrix.

^{13}C NMR spectra were acquired at 125.541 MHz using 1.0 s acquisition time, 27008.8 Hz spectral window, 8.1-8.6 μs (90°) pulse width, 3 s relaxation delay, and 1024 transients with WALTZ-16 modulated ^{1}H decoupling. ^{13}C T_1 relaxation time measurements were obtained at 125.541 MHz using a 27008.8 Hz spectral window, 8.1-8.6 μs (90°) pulse width, 1.0 s acquisition time, 60 s relaxation delay and 96 transients with 12 different d_2 delays (ranging from 0.0125-51.2 s) and WALTZ-16 modulated ^{1}H decoupling.

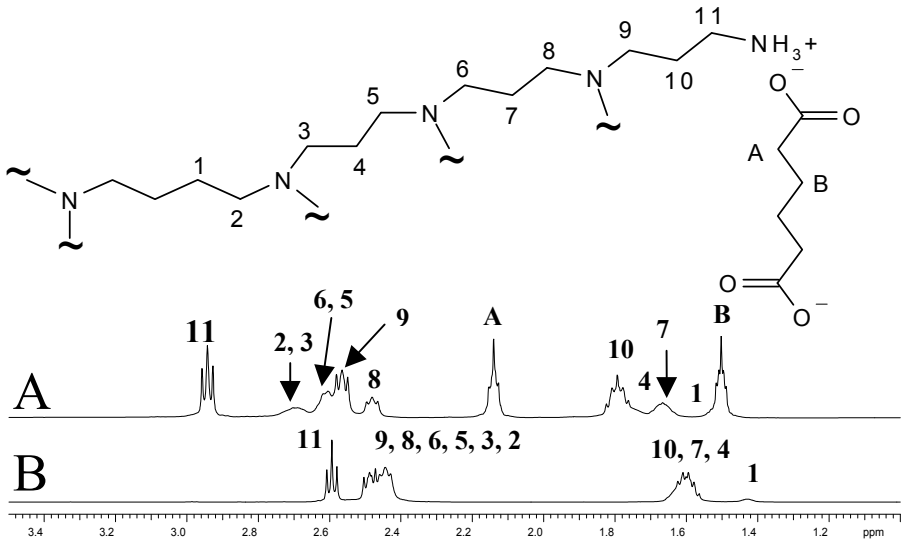

Figure 2.3. ^{1}H NMR spectra of PPI-3: (A) self-assembled with adipic acid and (B) alone.

Results and Discussion

^{1}H NMR spectra clearly showed the effect of self-assembly on the chemical shift of dendrimers and diacids. The ^{1}H NMR spectrum of PPI-3 alone in D_2O was poorly resolved (Figure 2.3B), making complete spectral assignment impossible. Upon self-assembly with diacids, the resonances of the PPI-3 moiety

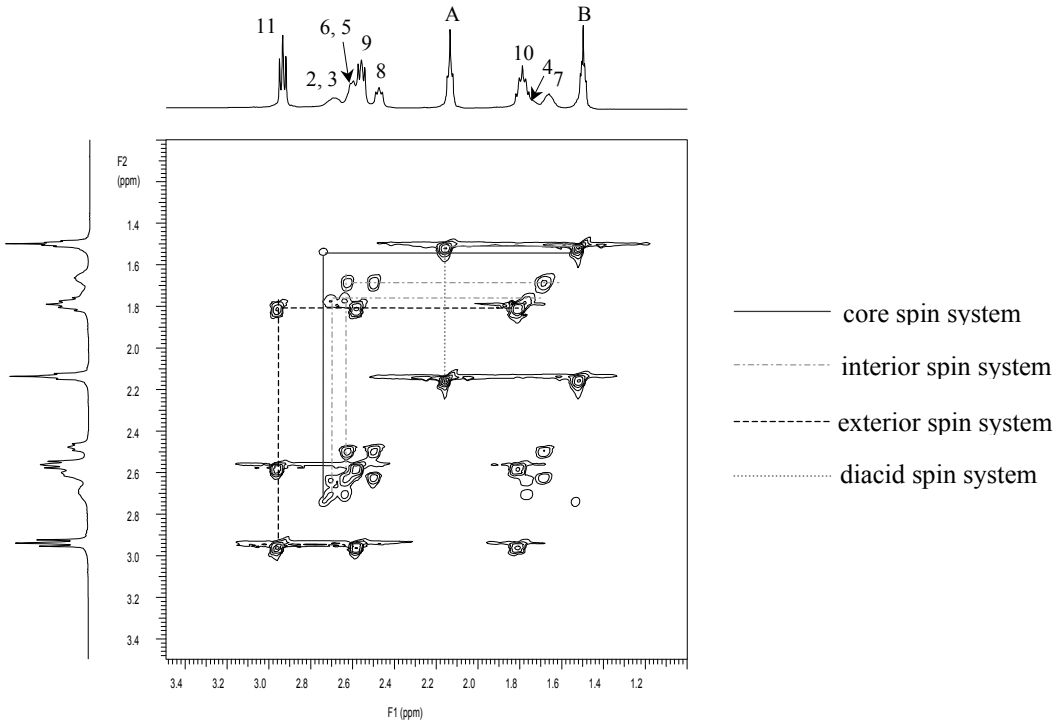

Figure 2.4. 2D TOCSY NMR spectrum of PPI-3 self-assembled with adipic acid.

became well resolved (Figure 2.3A). Combined with 2D TOCSY NMR spectrum (Figure 2.4), complete spectral assignment was achieved. In TOCSY, coupling between protons within an entire spin system is observed.[25] A closer examination of the PPI dendrimer shows several isolated spin systems within the molecule, separated by the nitrogen atoms of the tertiary amino groups. These spin systems correspond to the core, interior, and exterior of the dendrimer, and the diacid. Therefore, TOCSY was an attractive technique to obtain a complete spectra assignment for the dendrimer.

The observed increase in resolution of the dendrimer resonances was likely due to the formation of ion pairs between the dendrimers and diacids. These ion pairs would randomly tumble in solution, generating small, local magnetic fields that could affect the chemical shifts of the dendrimer protons. Differences were observed in the resolution of

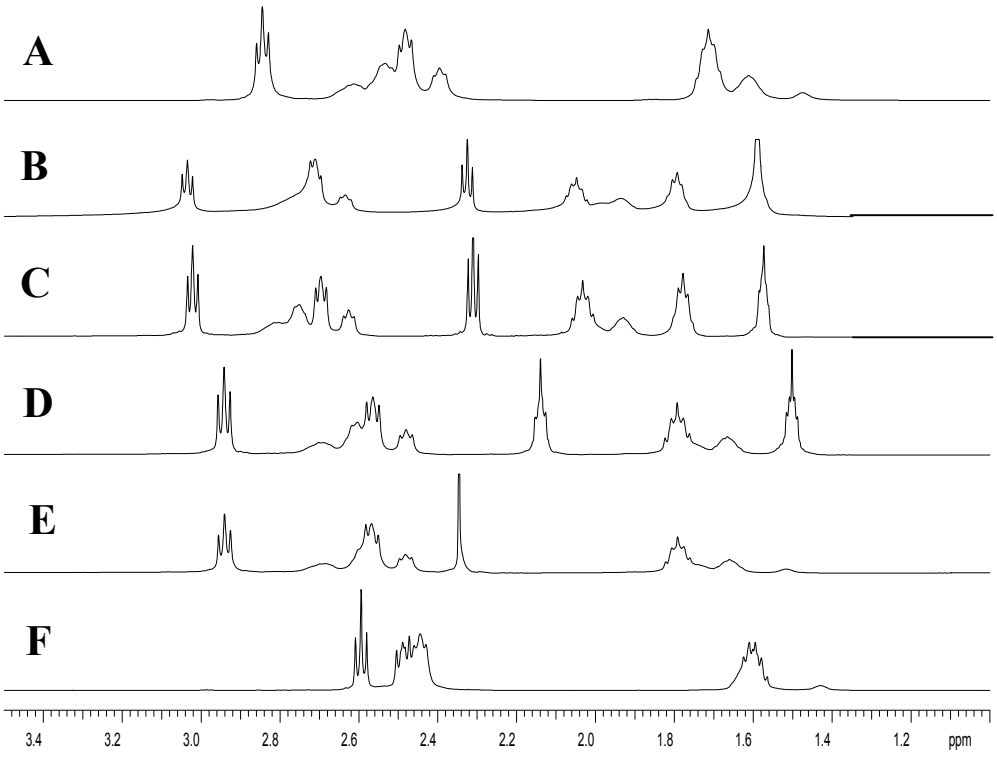

Figure 2.5. Stacked plots of ^{1}H NMR spectra of PPI-3 self-assembled with (A) phthalic acid; (B) sebacic acid; (C) suberic acid; (D) adipic acid; (E) succinic acid; (F) alone.

dendrimer peaks with changes in the diacid (Figure 2.5), suggesting that other interactions besides simple proton transfer occurred between diacids and dendrimers.

^{13}C NMR spectra of the PPI/diacid mixtures showed subtle changes in chemical shift compared with the NMR spectrum of PPI alone. Very little change was observed for the carbons of the PPI interior, while more noticeable changes were observed for the carbons of the PPI periphery, suggest that PPI/diacid acid interactions occur along the periphery of the dendrimer (Table 2.2). These changes in ^{13}C chemical shift can also be attributed to the formation of ion pairs between PPI and diacid moieties in the self-assemblies.

^{13}C T_1 relaxation time measurements were performed to gauge the effect of self-assembly on the carbon atoms of the dendrimer and diacid acids. T_1 relaxation involves the interactions of nuclei of a sample molecule with the other molecules in its local environment, such as solvent molecules or other sample molecules. These interactions are required for the nuclei to exchange energy with the environment and return to the Boltzman distribution. The shorter the T_1 relaxation time, the faster the energy exchange, and the stronger the interactions between nuclei.[25] Self-assembly of the dendrimers with

Table 2.2. Comparison of ^{13}C NMR Chemical Shifts and T_1 Values for PPI Dendrimers and Diacids Compared to Free PPI.

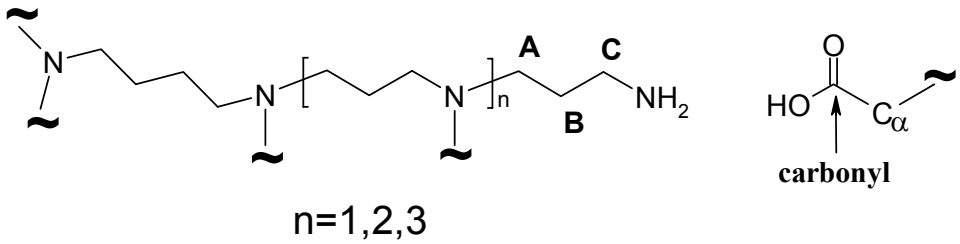

Sample	^{13}C Chemical Shifts (ppm)					^{13}C T_1 Values (sec)				
	Dendrimer			Dibasic Acid		Dendrimer			Dibasic Acid	
	A	B	C	carbonyl	α carbon	A	B	C	carbonyl	α carbon
PPI-2 alone	50.744	28.317	39.128	----------	----------	0.2382	0.3712	0.6329	----------	----------
+succinic	50.009	23.740	37.993	182.254	34.289	0.2364	0.3800	0.5669	13.14	1.806
+adipic	50.009	23.793	38.006	183.646	37.52	0.2527	0.3585	0.5332	12.95	0.9852
+suberic	50.140	24.308	38.153	184.079	37.697	0.2405	0.3617	0.5551	11.87	0.9148
+sebacic	50.019	23.783	38.002	184.092	37.753	0.2289	0.3011	0.5022	11.46	0.7913
+phthalic	49.992	23.714	37.996	177.418	137.807	0.2238	0.3233	0.5118	8.912	3.66
PPI-3 alone	50.741	28.304	39.128	----------	----------	0.2332	0.3580	0.5953	----------	----------
+succinic	50.051	23.770	38.045	182.152	34.355	0.1997	0.2911	0.4599	11.96	1.332
+adipic	50.009	23.688	38.006	183.485	37.572	0.2233	0.3240	0.4830	9.596	0.84
+suberic	50.002	23.632	37.989	183.836	37.753	0.1950	0.2908	0.4133	8.388	0.6228
+sebacic	50.058	23.721	38.012	183.771	37.812	0.2330	0.3682	0.5386	9.261	0.7847
+phthalic	49.996	23.691	38.019	177.303	137.928	0.2141	0.3187	0.4462	7.488	2.911
PPI-4 alone	50.800	28.383	39.191	----------	----------	0.2199	0.3283	0.5273	----------	----------
+succinic	50.009	23.711	38.006	182.021	34.348	0.1979	0.2795	0.4431	9.645	1.1
+adipic	49.940	23.603	37.943	183.324	37.569	0.1974	0.2692	0.3877	6.591	0.6217
+suberic	49.940	23.576	37.927	183.623	37.743	0.1986	0.2808	0.3809	6.621	0.5772
+sebacic	50.002	23.596	37.927	183.485	37.809	0.2031	0.2981	0.4000	6.124	0.5494
+phthalic	49.936	23.704	37.986	177.171	137.944	0.1879	0.2779	0.3805	5.065	1.974

diacids would dramatically increase the interactions between dendrimer and diacids. This increase in interactions would allow for faster exchange of energy. Consequently, reductions in the ^{13}C T_1 relaxation time of dendrimer and diacid carbons would occur. Decreases in ^{13}C T_1 values were observed for the terminal carbons of the dendrimer, as well as carbons of the diacid acids in the self-assembly (Tables 2.2). An inverse relationship was also observed between the generation of PPI and the length of the diacid for optimal self-assembly. For PPI-2, the self-assembly with sebacic acid gave the greatest reduction in ^{13}C T_1 values for the peripheral carbons of the dendrimer, indicating the most efficient self-assembly. For PPI-3, suberic acid is the best acid for self-assembly. For PPI-4, adipic acid is the optimal diacid for self-assembly. Comparisons of the T_1 values of diacids with different dendrimers was not made because of differences in concentration of the diacids with different generations of PPI (Table 2.1).

Formation of the self-assemblies is likely a two-step process. First, one proton is transferred from one of the carboxylic acid groups of the diacid to the primary amine group of the dendrimer to form an ion pair. This association "tethers" the acid to the dendrimer. In the second step, another proton transfers from another carbonyl group to the dendrimer's amino group to form a second ion pair (Figure 2.6). Therefore, the entropy of the process favors the intramolecular self-assembly between diacid and the two primary amino groups of the dendrimer. This effect is similar to the chelate effect observed in coordination chemistry.[26]

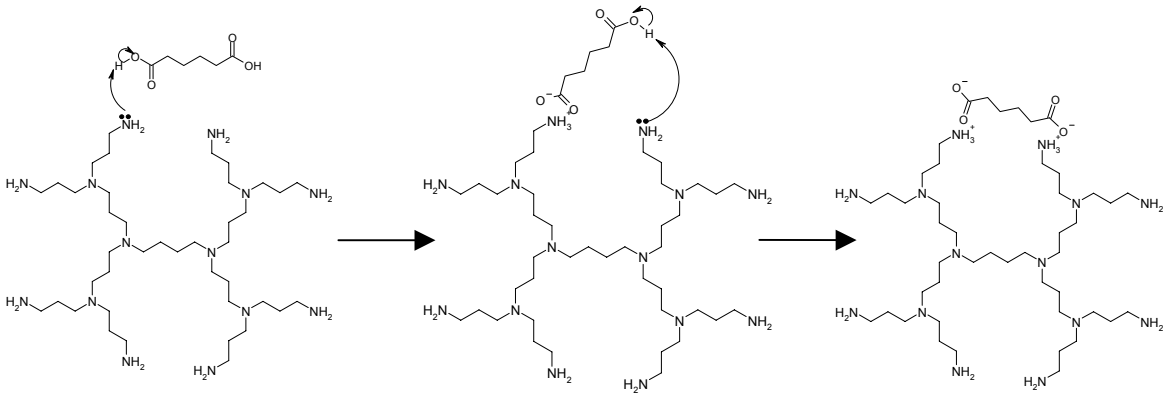

Figure 2.6. Scheme for the formation of PPI/diacid self-assembly.

Previous studies have shown that dendrimers like PPI have extended chain conformations in polar solvents, which can maximize dendrimer/solvent interactions and results in well-separated dendritic arms.[27] In order to form stable PPI/diacid self-assemblies, the length of the diacid must be complimentary to the extended conformations of the dendritic chains to maximize electrostatic interactions. Steric hindrance occurs for the dendritic chains of higher generation dendrimers because of the increased number of end groups along the periphery. As a result, smaller diacids can accommodate higher generation dendrimers to form the most efficient self-assemblies. The observed changes in ^{1}H and ^{13}C NMR spectra and ^{13}C T_1 values clearly demonstrate that self-assemblies have been formed between PPI dendrimers and diacids.

Conclusions

Self-assemblies of PPI dendrimers and diacids can be formed in aqueous solutions. Formation of self-assemblies showed great increases in resolution in dendrimer ^{1}H NMR spectra, allowing for a complete spectral assignment of the

dendrimer resonances. Variations in ^{1}H and ^{13}C spectra have been observed for dendrimers with different diacids, indicating differences in the interactions between dendrimers with different diacids. Reductions in ^{13}C T_1 relaxation times indicated that self-assembly formed between dendrimer and diacid, and showed an inverse relationship between the generation off dendrimer and the size of the diacid for self-assembly (with an increase in the generation of dendrimer, a smaller diacid is needed for optimal self-assembly).

Chapter 3: Encapsulation of Fluorescent Dyes Within PPI/Diacid Acid Self-Assemblies

Introduction

As mentioned in Chapter 1, the hyperbranched and spherical structure of dendrimers results in the presence of void spaces within the interior of dendrimers.[1,2,9] These dendritic voids give dendrimers the ability to encapsulate many types of small guest molecules. This, combined with the ease of modification to tune their properties, gives dendrimers the capability to be excellent encapsulation agents for diverse applications.[10,11]

A particularly promising application of dendrimers is drug delivery. Takagishi *et al*[28] reported the encapsulation of the anticancer drugs adriamycin (ADR) and methotrexate (MTX) within poly(ethylene glycol) modified PAMAM dendrimers. Modification of the dendrimers was performed to reduce their cytotoxicity. These modified dendrimers were able to encapsulate MTX much more strongly and release it much more slowly than ADR due to stronger electrostatic interactions between MTX and the dendrimer.

Light-harvesting and energy transfer is another interesting application of dendrimers. Meijer *et al*[29] synthesized a series of PPI dendrimers modified at the periphery with π-conjugated oligo(*p*-phenylene vinylene) (OPV) groups. It was found that these dendrimers can form stable monolayers at the air-water interface and can encapsulate anionic dyes and transfer them from aqueous to organic layers. When the OPV units were excited at 420 nm, their fluorescence was quenched, and emission of the

encapsulated dyes occurred, indicating energy transfer. Addition of a dye/OPV dendrimer to thin films of poly(phenylene vinylene) (PPV) showed energy transfer from polymer to dye. These systems provide an excellent approach for adjusting the emission wavelength of conductive polymers and have potential in use in polymer light-emitting diodes.

Another important application of dendrimers is their use as recyclable solubilizing agents. Fréchet *et al*[30] synthesized a poly(ether) dendrimer from a 3,5-hydroxybenzyl alcohol monomer with a carboxylic acid periphery, resulting in a molecule with a nonpolar interior and a polar periphery. This dendrimer acts as a unimolecular micelle, and was used to dissolve hydrophobic molecules like pyrene into water at much higher concentrations than pyrene alone. Acidifying the solution results in the precipitation of the dendrimer/pyrene system. Dissolving the system in an organic solvent releases the hydrophobic molecule into the solvent, and treatment with aqueous base transfers the dendrimer to the aqueous phase. Another example of a unimolecular micelle was reported by Newkome *et al.*[31] A saturated hydrocarbon dendrimer with a carboxylic acid periphery was used to dissolve the micellar probes phenol blue and pinacyanol chloride in water.

A novel approach of dendrimers as solubilizing agents has been conducted by modifying the periphery of polar dendrimers with nonpolar functional groups to form inverse dendritic unimolecular micelles. Meijer *et al*[32] reported the modification of different generations of PPI dendrimers with palmitoyl chloride to form inverse micelles. These dendrimers were able to extract various hydrophilic xanthene dyes into organic solvents.

Non-covalent interactions have been used to form self-assembled inverse micelles. Crooks *et al*[24] reported the formation of inverse micelles through the spontaneous self-assembly of PAMAM dendrimers and dodecanoic acid by electrostatic interactions. This inverse micelle can shuttle hydrophilic dyes between polar and nonpolar phases based on the pH sensitivity of the self-assembly.

Self-assemblies between dendrimers and diacids can offer a unique system for the encapsulation of guest molecules, which can potentially be used in drug delivery or as nanoreaction vessels. Once self-assembly between PPI dendrimers and diacids was established (see Chapter 2), investigations on the encapsulation properties of these self-assemblies were performed. In this project, encapsulation of different fluorescent dyes (Figure 3.1) within self-assemblies of PPI dendrimers (generations 3, 4, and 5) (Figure 1.3) and diacids (Figure 3.2) was studied. Different generations of PPI and different diacids were used to optimize relationships between dendrimer, acid, and encapsulation of dyes. UV-vis, fluorescence, and NMR spectroscopies were used to probe changes in the dyes upon addition of PPI and formation of the self-assembly.

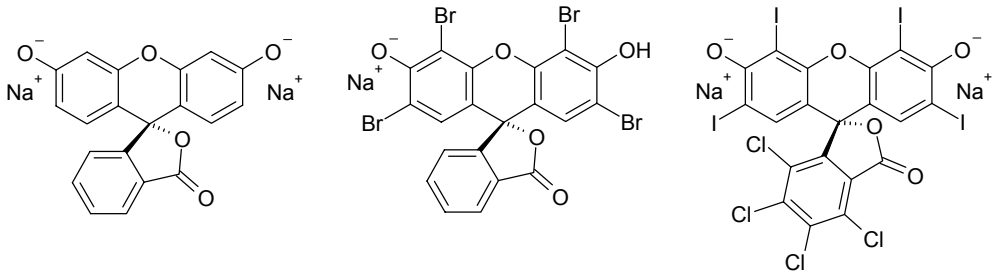

Figure 3.1. Structures of fluorescent dyes used in this study.

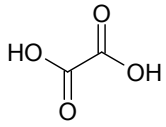

oxalic acid

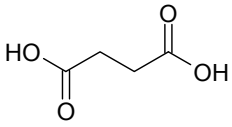

succinic acid

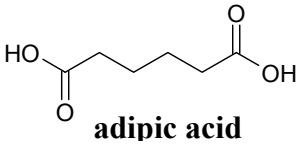

adipic acid

Figure 3.2. Structures of diacids used in this study.

Experimental

General

Poly(propylene imine) dendrimers and rose bengal were obtained from Aldrich Chemical Company. Adipic acid was obtained from Lancaster Synthesis. Succinic and oxalic acids were obtained from Fisher Scientific, Inc. Fluorescein was obtained from Central Chemical Company and eosine y from Merck and Co. Deuterium oxide was obtained from Norrell, Inc. All chemicals were used as received without further purification. All solutions were prepared in deionized water. The pH of dye solutions was adjusted to 8.0 using 0.1M HCl and 0.1M NaOH. All pH measurements were made using IQ Scientific Instruments pH/mV/temp meter (model IQ150). Concentrations of all reagents used for UV-vis and fluorescence spectroscopies are summarized in Table 3.1.

Table 3.1. Concentrations of Reagents for UV-vis and Fluorescence Spectroscopies.

Compound	Concentration (M)	
	UV-vis	***Fluorescence***
fluorescein	3.45×10^{-5}	5.00×10^{-8}
eosine yellowish	1.02×10^{-5}	5.00×10^{-8}
rose bengal	8.02×10^{-6}	5.00×110^{-8}
PPI-3	0.0101	1.00×10^{-5}
PPI-4	0.00519	1.00×10^{-5}
PPI-5	0.01	1.00×10^{-5}
ethylenediamine	0.0113	0.001
adipic acid	0.0503	0.001
succinic acid	0.0529	0.001
oxalic acid	0.0597	0.001

UV-vis Spectroscopy

All UV-vis spectra were obtained at 25°C using a Hewlett-Packard 8452A diode-array spectrophotometer. Dye solution (2 mL) was added to a 1-cm quartz cuvet, followed by PPI dendrimer and a stoichiometric amount of diacid (8:1 diacid-to-PPI-3, 16:1 diacid-to-PPI-4, 32:1 diacid-to-PPI-5). A 2:1 molar ratio of PPI-to-dye was maintained so that all dye molecules were expected to be encapsulated (Figure 3.3). UV-vis spectra were obtained after each addition using a water blank. Solutions of fluorescein with the PPI-3/adipic acid self-assembly were prepared at different pH values to investigate the effect of pH on encapsulation.

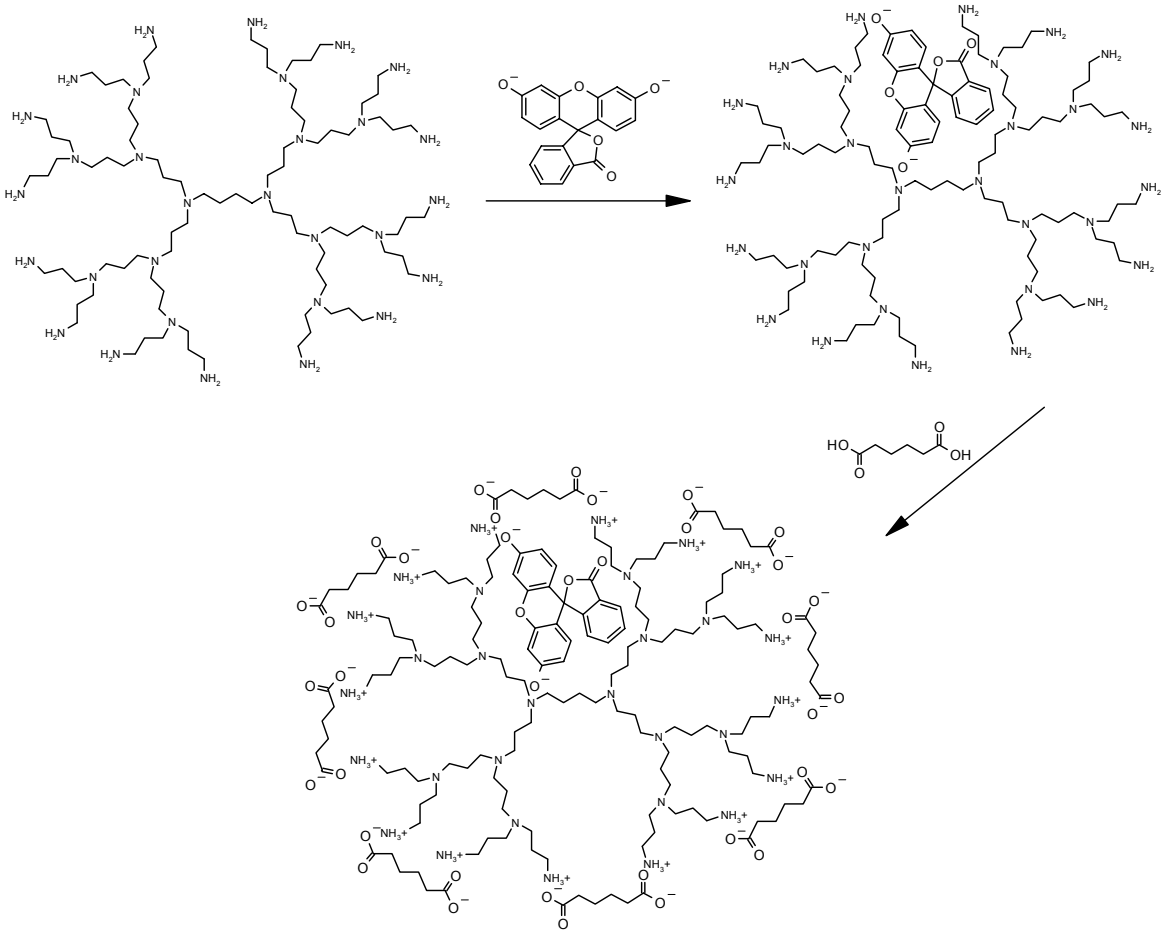

Figure 3.3. Scheme for encapsulation of fluorescein within PPI-3/adipic acid self-assembly.

Fluorescence Spectroscopy

All fluorescence spectra were obtained at 25°C using a SPEX Fluorolog III lifetime fluorimeter equipped with a temperature control sample holder. Dye solution (2 mL) was added to a 1-cm quart cuvet, followed by 20 μL of PPI solution and a stoichiometric amount of diacid. Emission spectra were acquired after each addition. The following excitation wavelengths were used: 480 nm for fluorescein; 516 nm for eosine y; and 540 nm for rose bengal.

For UV-vis and fluorescence studies, control experiments using ethylenediamine and adipic acid were performed for each dye to determine the effect of a classical amine on the properties of the dyes. Ethylenediamine concentration was adjusted to match the primary amine concentration of PPI-3 used in the study.

NMR spectroscopy

NMR samples of fluorescein, fluorescein/PPI-3, and fluorescein/PPI-3/adipic acid were prepared using 0.7 mL D_2O in 5 mm NMR tubes. A 3:1 molar ratio of fluorescein-to-PPI-3 was maintained to ensure sufficient signal for fluorescein. All spectra were collected at ambient temperature on a 4-channel Varian UnityPlus 500 MHz NMR spectrometer equipped with a Nalorac triple resonance PFG $^{1}H/^{13}C/X$ probe (X tunable from ^{15}N to ^{31}P) and a Varian broadband probe. D_2O was used as an internal reference for all ^{1}H spectra, and ^{13}C spectra were externally referenced with TMS in D_2O using a concentric NMR tube. All NMR data were processed using Varian VNMR software on a SUN UltraSPARC-60 workstation.

^{1}H spectra of all samples were acquired at 499.220 MHz using a 4706.4 Hz spectral window, 5.5 μs (60°) pulse width and 64 transients. 2D ^{1}H-^{1}H NOESY spectra

were acquired at 499.220 MHz using a 4706.4 Hz spectral window, 1 s mixing time, 8.9-9.3 μs (90^o) pulse width, a 2 s relaxation delay and 0.5 s acquisition time. 16 transients were averaged for each 2x400 complex t_1 increments. Data processing was performed with Gaussian weighting in both dimensions and zero filling to display the data on a 4096x1024 two-dimensional matrix.

^{13}C spectra were obtained at 125.541 MHz using a 27008.8 Hz spectral window, 1.0 s acquisition time, 5.8-6.1 μs (90^o) pulse width, 3 s relaxation delay, 1024 transients, and WALTZ-16 modulated ^1H decoupling. ^{13}C T_1 relaxation time measurements were performed using a 27008.8 Hz spectral window, 1.0 s acquisition time, 5.8-6.1 μs (90^o) pulse width, 60 s relaxation delay and 96 transients with 12 different d2 delays (ranging from 0.0125-51.2) and WALTZ-16 modulated ^1H decoupling.

Results and Discussion

NMR spectroscopy was used to probe the encapsulation of fluorescein in PPI-3 and the PPI-3/adipic acid self-assembly. For fluorescein alone in D_2O, the ^1H NMR spectrum (Figure 3.4C) showed good resolution. Reductions in resolution of the fluorescein peaks were observed when in the presence of PPI-3 (Figure 3.4B). The peaks of protons **d** shifted downfield to overlap with those of **c** and **c'** and the peaks of protons **a** and **a'** shifted downfield to overlap with those of **b** and **b'**. Upon the self-assembly of PPI-3 and adipic acid, the resolution of the ^1H NMR spectrum was improved (Figure 3.4A), however, chemical shifts for protons **b**, **b'**, **d**, **d'**, **e**, and **f** showed subtle, but noticeable, changes compared to the spectrum of fluorescein alone.

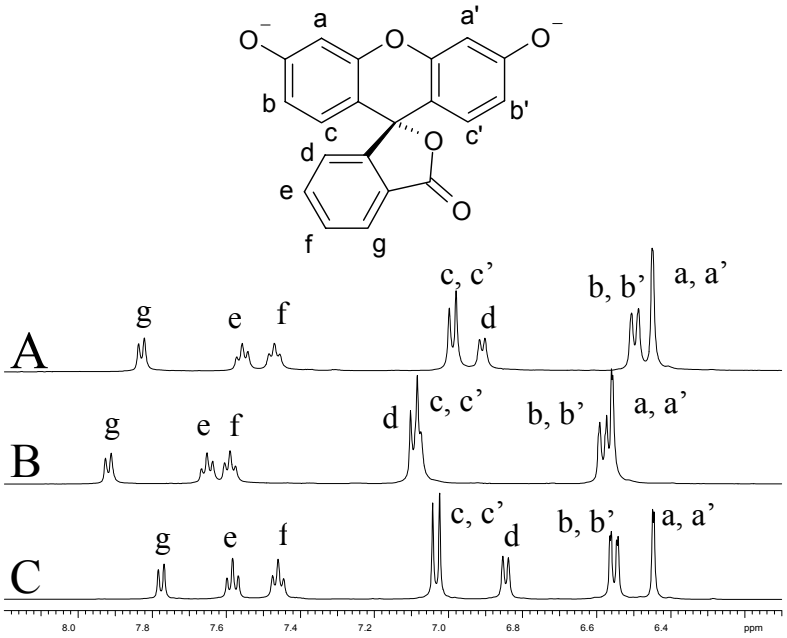

Figure 3.4. 1D ^{1}H NMR spectra of fluorescein: (A) with PPI-3/adipic acid self-assembly; (B) with PPI-3; (C) alone.

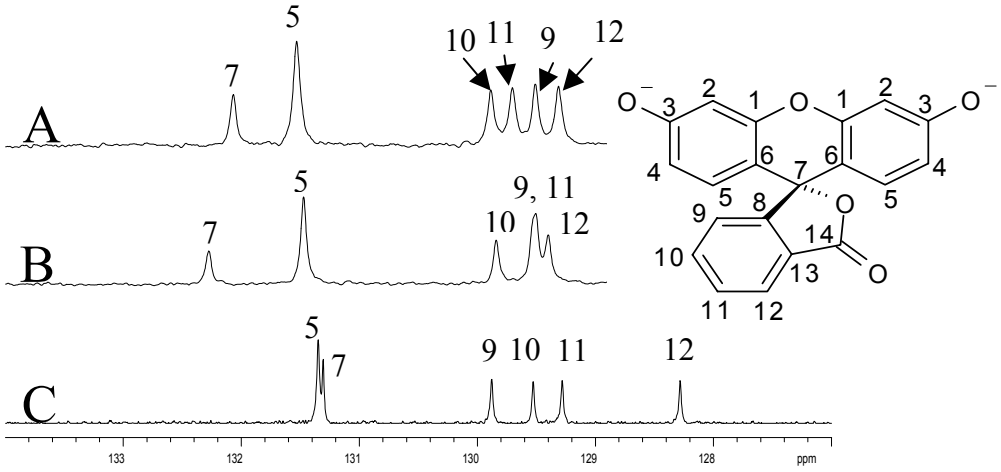

Figure 3.5. 1D ^{13}C NMR spectra of fluorescein: (A) with PPI-3/adipic acid self-assembly; (B) with PPI-3; (C) alone.

^{13}C NMR spectra of fluorescein also displayed changes in chemical shift in the presence of PPI-3 or PPI-3/adipic acid self-assembly. Quantitative ^{13}C NMR and HETCOR spectra (see Appendix 2) further indicated overlap occurred for the peaks of carbons **5** and **7** for fluorescein alone (Figure 3.5C). Upon addition of PPI-3 (Figure

3.5B), there were significant downfield shifts for carbons **7** and **12** and peaks for carbons **9** and **11** were overlapped with addition of PPI-3. However, addition of adipic acid resolved these peaks (Figure 3.5A). There are two potential explanations for the observed changes in the ^{1}H and ^{13}C NMR spectra for fluorescein: (1) a dramatic change in the local chemical environment of the dye; or (2) a change in the structure of the dye. The significant downfield shift of carbon **7** suggested a change in the hybridization of this carbon from sp^3 to sp^2 upon addition of PPI-3 and formation of the PPI-3/adipic acid self-assembly.

For the dianion form of fluorescein and derivatives, there are two types of structures in equilibrium: a lactone and a carboxylate (Figure 3.6). Carbon **7** can have sp^3 hybridization (lactone form) or sp^2 hybridization (carboxylate form). The carboxylate has a higher degree of conjugation than the lactone, which may explain the changes in ^{13}C chemical shift.

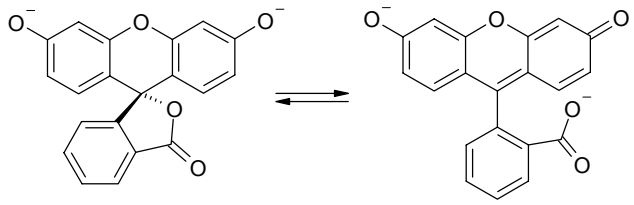

lactone carboxylate

Figure 3.6. Equilibrium of lactone and carboxylate structures for dianion of fluorescein.

^{13}C T_1 relaxation measurements were also used to investigate encapsulation of fluorescein. Because energy transfer for nuclear spins through spin-lattice (T_1) relaxation to return to a Boltzmann distribution is dependent upon the surroundings of the sample molecules,[25] a comparison of the T_1 values of fluorescein with PPI-3 and the PPI-3/adipic

acid self-assembly can give information about the interactions of fluorescein with the dendrimer and self-assembly. All ^{13}C T_1 values for fluorescein are summarized in Table 3.2. Except for carbon **7**, there were reductions in T_1 values for all carbons upon addition of PPI-3, due to encapsulation of fluorescein within the interior of PPI-3. Carbon 7 had a significant increase in T_1, however, because of changes in hybridization from sp^3 to sp^2. When alone in solution, carbon **7** of fluorescein is sp^3 hybridized (lactone form). When encapsulated with PPI-3 or self-assembly, fluorescein dianions may prefer the carboxylate form in solution due to the flexibility of the structure, which can better adapt to the restricted dendritic voids. This change in hybridization reduces the ability of carbon 7 to transfer magnetization among other atoms, resulting in an increase in T_1 relaxation time. In general, the T_1 values for the carbons of fluorescein were reduced further when encapsulated within the PPI-3/adipic acid self-assembly.

Table 3.2. ^{13}C Chemical Shift and T_1 Values for Fluorescein Alone, with PPI-3, and with PPI-3/Adipic Acid Self-Assembly.

Carbon	^{13}C Chemical Shift (δ)			^{13}C T_1 Values (s)		
	fluorescein	fluorescein/ PPI-3	fluorescein/ PPI-3/adipic	fluorescein	fluorescein/ PPI-3	fluorescein/P PI-3/adipic
1	158.553	158.743	158.487	2.1420	1.1060	1.0670
2	103.793	103.931	103.951	0.3617	0.2682	0.2933
3	180.507	180.993	180.773	1.4370	1.0020	0.8101
4	122.957	123.387	123.331	0.3220	0.2440	0.2410
5	131.447	131.473	131.532	0.3119	0.2161	0.2132
6	112.287	112.034	111.929	2.2270	1.0110	0.9687
7	131.447	132.274	132.068	0.3119	1.0020	0.6048
8	158.983	159.265	159.456	1.8790	0.7483	0.7288
9	129.953	129.845	129.884	0.3538	0.2522	0.2137
10	129.595	129.513	129.704	0.3237	0.2443	0.2541
11	129.352	129.513	129.51	0.3987	0.2443	0.2397
12	128.433	129.398	129.313	0.3607	0.2345	0.2634
13	139.599	139.937	139.494	2.0610	0.9674	1.0420
14	175.221	173.98	173.803	4.4860	2.7300	1.9610

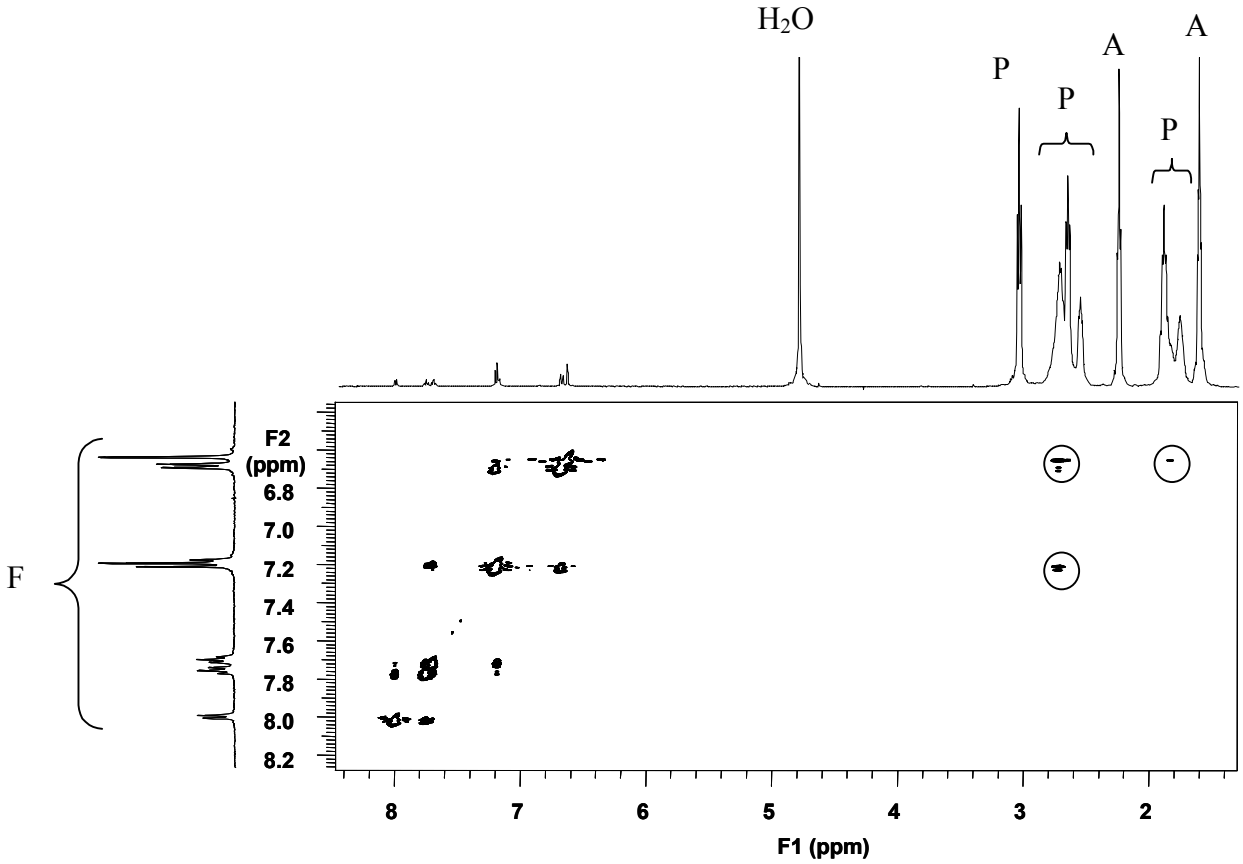

A – acid moiety; F – Fluorescein; P – PPI-3 moiety

Figure 3.7. 2D ^{1}H-^{1}H NOESY spectrum of fluoresecin with PPI-3/adipic acid self-assembly.

2D NOESY (**N**uclear **o**verhauser **e**ffect **s**pectroscop**y**) was used to confirm encapsulation of fluorescein with the PPI-3/adipic acid self-assembly. In NOESY, transfer of magnetization between nuclear spins occurs by through-space interactions (dipole-dipole interactions) which also aids in the relaxation of the nuclei to the Boltzmann distribution.[33] A measure of these interactions can be used to determine the spatial relationship between nuclei within a molecule or between different molecules. NOE cross-peaks between protons **a**, **a'**, **b**, **b**', **c**, **c'**, and **d** of fluorescein with the interior protons of PPI-3 in the PPI-3/adipic acid self-assembly were observed in the 2D NOESY

spectrum (Figure 3.7). This result indicated encapsulation of fluorescein within the PPI-3/adipic acid self-assembly.

The UV-vis spectrum of fluorescein alone in aqueous solution had a λ_{max} at 490 nm. Addition of PPI-3 resulted in a red shift of λ_{max} to 492 nm. A further red shift of λ_{max} to 498 nm was observed upon addition of adipic acid to the fluorescein/PPI-3 mixture (Figure 3.8). Similar results were obtained using succinic and oxalic acids (Table 3.3). The final pH of the reaction mixtures ranged from about 7.5-8.0. At this pH range, the dianion of fluorescein (phenolate ion form) is the prevalent species, with a λ_{max} at 490 nm.[34,35] The red shift in the UV-vis spectra of fluorescein was likely due to a change in the solvation of the dye molecule upon addition of PPI-3 and formation of the self-assembly, rather than changes in pH. UV-vis spectra of fluorescein with ethylenediamine and adipic acid in the control experiment confirmed this reasoning

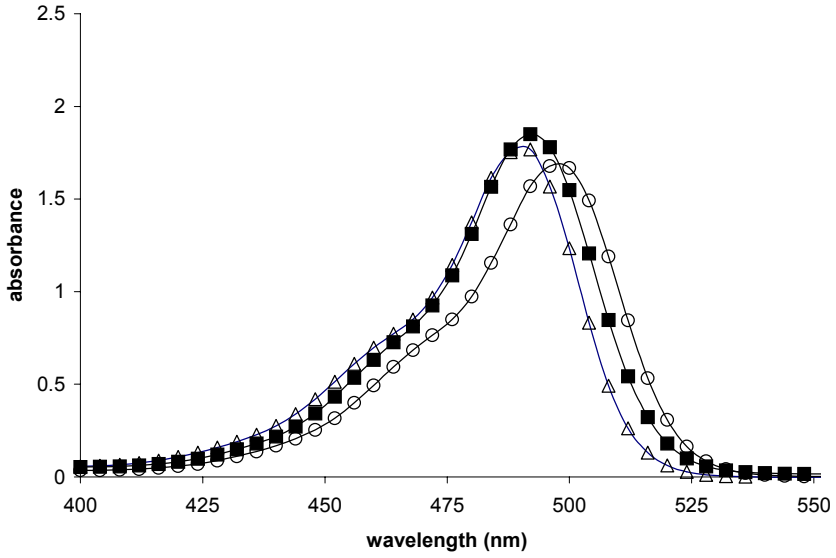

Figure 3.8. UV-vis spectra of fluorescein: (Δ) alone; (■) with PPI-3; (○) with PPI-3/adipic acid self-assembly.

Table 3.3. λ_{max} and Absorbance Values in the UV-vis Spectra for Fluorescent Dyes in the Presence of Different PPI/Diacid Acid Self-Assemblies.

Dendrimer	Sample	UV-vis l_{max} (nm) (absorbance)								
		Fluorescein			Eosine Yellowish			Rose Bengal		
		oxalic acid	succinic acid	adipic acid	oxalic acid	succinic acid	adipic acid	oxalic acid	succinic acid	adipic acid
PPI-3	dye alone	490 (1.7552)	490 (1.7293)	490 (1.7760)	516 (0.6977)	516 (0.6633)	516 (0.6569)	548 (0.6816)	548 (0.6633)	548 (0.6984)
	+dendrimer	492 (1.9030)	492 (1.8406)	492 (1.8496)	524 (0.6293)	524 (0.6145)	524 (0.6702)	560 (0.4860)	560 (0.5337)	560 (0.5573)
	+acid	498 (1.8346)	498 (1.8057)	498 (1.6916)	524 (0.6316)	524 (0.5994)	524 (0.6028)	560 (0.4125)	560 (0.4599)	560 (0.4446)
PPI-4	dye alone	490 (1.7564)	490 (1.7658)	490 (1.7333)	516 (0.6674)	516 (0.6606)	516 (0.6568)	550 (0.6627)	550 (0.6580)	548 (0.6719)
	+dendrimer	494 (1.7440)	496 (1.7231)	494 (1.7739)	526 (0.6770)	526 (0.6874)	526 (0.6686)	562 (0.6348)	562 (0.6496)	562 (0.6586)
	+acid	500 (1.7983)	500 (1.7569)	500 (1.7294)	526 (0.6274)	524 (0.6220)	526 (0.6029)	562 (0.5870)	562 (0.5950)	562 (0.5635)
PPI-5	dye alone	490 (1.7615)	490 (1.7466)	490 (1.7579)	516 (0.6413)	516 (0.6445)	516 (0.6559)	550 (0.6569)	550 (0.6513)	550 (0.6540)
	+dendrimer	500 (1.7232)	498 (1.7498)	498 (1.7394)	528 (0.6981)	528 (0.6792)	528 (0.6718)	562 (0.6528)	562 (0.6546)	562 (0.6436)
	+acid	502 (1.8317)	502 (1.7429)	502 (1.7429)	528 (0.6320)	528 (0.6277)	528 (0.6071)	562 (0.6116)	562 (0.6077)	562 (0.5822)

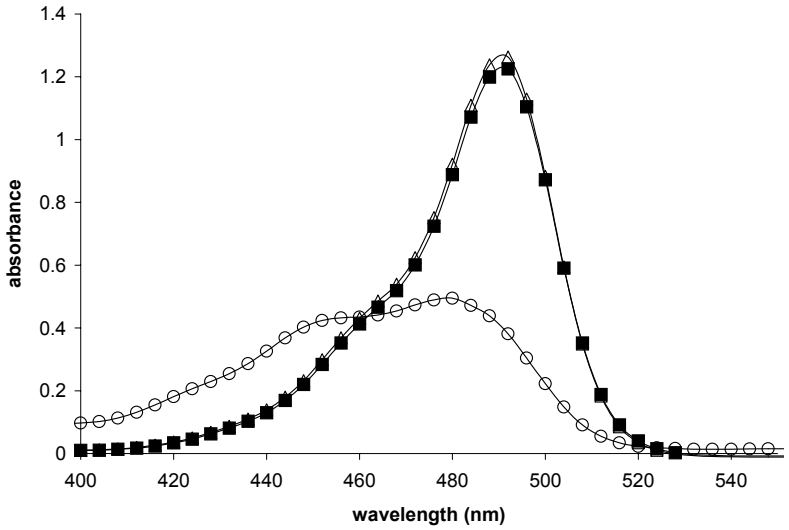

Figure 3.9. UV-vis spectra of fluorescein: (Δ) alone; (■) with ethylenediamine; (○) with ethylenediamine and adipic acid.

(Figure 3.9). Addition of ethylenediamine caused no change in either λ_{max} or absorbance. Addition of adipic acid resulted in a significant blue shift in the spectrum due to reduction in pH upon addition of the acid, causing the formation of the neutral species of fluoresein (the phenol form).

Red shifts of λ_{max} in the UV-vis spectra of fluorescein were also observed using PPI-4 and PPI-5 and their self-assemblies with diacids (Table 3.3). There was an

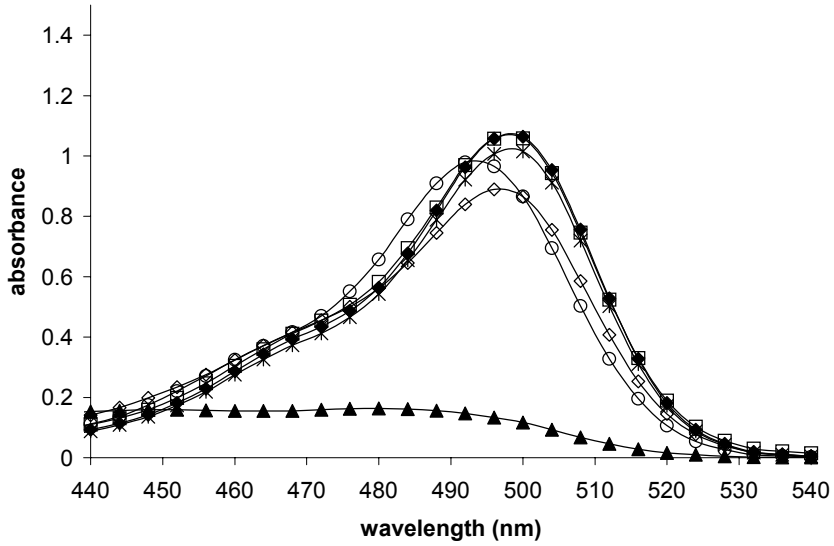

Figure 3.10. UV-vis spectra of fluorescein with PPI-3/adipic acid self-assembly at different pH: (▲) 4.14; (✧) 6.03; (□) 6.93; (◆) 8.00; (*) 9.08; (O) 9.98.

increase trend in the red shift of λ_{max} with increasing generation of dendrimers (λ_{max} = 494 nm for PPI-,4 and λ_{max} = 498 nm for PPI-5). Intermediate red shifts of λ_{max} were not observed for eosine y and rose bengal (Table 3.3).

UV-vis spectra of fluorescein with PPI-3 and adipic acid at different pH (Figure 3.10) were obtained to gain information about the pH effect on encapsulation. At acidic pH, λ_{max} was at 480 nm and at strongly basic pH, λ_{max} = 496 nm. At a pH range of 7.00-9.00 (neutral to weakly basic), λ_{max} =498 nm; only changes in absorbance were observed, with a maximum absorbance at pH = 8.00. A further increase in pH to 9.98 caused a blue shift of λ_{max} to 494 nm. These results indicated that at neutral and weakly basic pH, the self-assembly was stable, with fluorescein entrapped inside the "interlocked" self-assembly. The self-assembly was open to solvent, affecting the absorbance properties of the dye. At extremely acidic or basic pH, the "interlocked" structure of the self-assembly was broken, with subsequent free migration of the dye in and out of the dendritic voids.

As dye molecules are partitioned into the relatively nonpolar interior of the dendrimer, the solvation of the dye molecules changes. This difference in solvation results in changes in the energies of the electronic orbitals of the dye molecules. A reduction in the energy difference between the bonding π and anti-bonding π^* orbitals results in a slight red shift in the UV-vis spectrum.[36] This, combined with the NMR evidence, suggests that there is a change in solvation of the dye, as well as a change in conjugation of the dye, upon encapsulation of the dye within the PPI/diacid self-assembly.

Changes in the UV-vis spectra of the dyes in the presence of ethylenediamine and adipic acid were consistent with changes in the pH of the system, confirming encapsulation of the dyes within the PPI/diacid self-assemblies.

Fluorescence spectroscopy was used to monitor changes in the fluorescence properties of the dyes encapsulated inside the self-assembly of PPI and diacids. There was a 40% reduction in fluorescence of fluorescein upon addition of PPI-3, and addition of adipic acid caused a further 23% reduction in fluorescence (Figure 3.11). Succinic and oxalic acids were also used for the fluorescence study, as well as PPI-4 and PPI-5 (Table 3.4). Reductions in fluorescence were also observed for eosine y and rose bengal (Table 3.4), however, the intermediate reductions were much smaller than those for fluorescein. In the control tests using fluorescein with addition of ethylenediamine and adipic acid (Figure 3-12), fluorescence reductions were observed, although, these reductions were much smaller than those of fluorescein in the

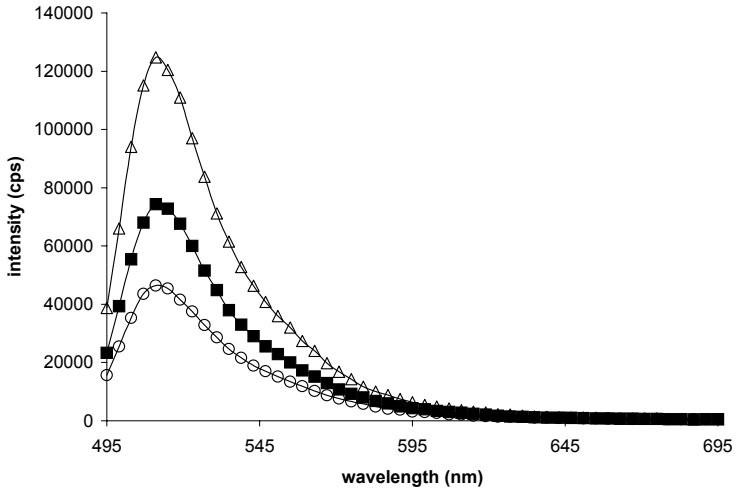

Figure 3.11. Fluorescence spectra of fluorescein: (Δ) alone; (■) with PPI-3; (○) with PPI-3/adipic acid self-assembly .

Table 3.4. Fluorescence Emission Intensities of Fluorescent Dyes with Different PPI/Diacid Self-Assemblies

Dye	Sample	UV-vis λ_{max} (absorbance)								
		PPI-3			PPI-4			PPI-5		
		oxalic acid	succinic acid	adipic acid	oxalic acid	succinic acid	adipic acid	oxalic acid	succinic acid	adipic acid
fluorescein	dye alone	490 (1.7552)	490 (1.7293)	490 (1.7760)	490 (1.7564)	490 (1.7658)	490 (1.7333)	490 (1.7615)	490 (1.7466)	490 (1.7579)
	+dendrimer	492 (1.903)	492 (1.8406)	492 (1.8496)	494 (1.744)	496 (1.7231)	494 (1.7739)	500 (1.7232)	498 (1.7498)	498 (1.7394)
	+acid	498 (1.8346)	498 (1.8057)	498 (1.6916)	500 (1.7983)	500 (1.7569)	500 (1.7294)	502 (1.8317)	502 (1.7429)	502 (1.7429)
eosine y	dye alone	516 (0.6977)	516 (0.6633)	516 (0.6569)	516 (0.6674)	516 (0.6606)	516 (0.6568)	516 (0.6413)	516 (0.6445)	516 (0.6559)
	+dendrimer	524 (0.6293)	524 (0.6145)	524 (0.6702)	526 (0.6770)	526 (0.6874)	526 (0.6686)	528 (0.6981)	528 (0.6792)	528 (0.6718)
	+acid	524 (0.6316)	524 (0.5994)	524 (0.6028)	526 (0.6274)	524 (0.6220)	526 (0.6029)	528 (0.6320)	528 (0.6277)	528 (0.6071)
rose bengal	dye alone	548 (0.6816)	548 (0.6633)	548 (0.6984)	550 (0.6627)	550 (0.6580)	548 (0.6719)	550 (0.6569)	550 (0.6513)	550 (0.6540)
	+dendrimer	560 (0.4860)	560 (0.5337)	560 (0.5573)	562 (0.6348)	562 (0.6496)	562 (0.6586)	562 (0.6528)	562 (0.6546)	562 (0.6436)
	+acid	560 (0.4125)	560 (0.4599)	560 (0.4446)	562 (0.5870)	562 (0.5950)	562 (0.5635)	562 (0.6116)	562 (0.6077)	562 (0.5822)

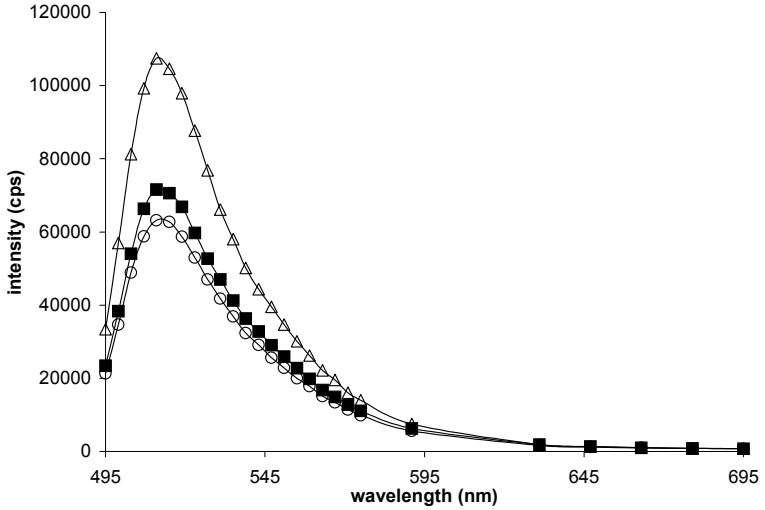

Figure 3.12. Fluorescence spectra of fluorescein: (Δ) alone; (■) with ethylenediamine; (○) with ethylenediamine and adipic acid.

PPI/diacid self-assemblies, suggesting interactions of fluorescein with self-assemblies were stronger than those with ethylenediamine/adipic acid. This also implied that the dye molecules were restricted within the dendritic voids through the interlocked self-assembly between dendrimers and diacid acids.

PPI dendrimers have many tertiary amino groups within the interior and primary amino groups along the periphery. Amines are excellent fluorescence quenchers.[37] When the dyes are partitioned into the restricted dendritic voids of the dendrimers, they are in close proximity to the tertiary amines, which enhances the efficiency of fluorescence quenching because quenching depends on the random collisions between dye and amine. A similar trend was observed in fluorescence emission with the generation of dendrimer compared with the UV-vis studies. When in the presence of ethylenediamine, fluorescence quenching was less efficient. More free motion of the dyes leads to fewer encounters with the quenching agents.

Conclusions

The fluorescent dyes fluorescein, eosine y, and rose bengal (Figure 3.1) were encapsulated within self-assemblies of PPI dendrimers (Figure 1.3) and diacids (Figure 3.2). NMR spectroscopy indicated encapsulation of fluorescein within the PPI-3/adipic acid self-assembly. ^{1}H and ^{13}C NMR sugggested that changes in the local environment (change in solvation) around the dye molecules occurred upon formation of the self-assembly, as well as a change in the structure of the dye upon encapsulation (leading to an increase in conjugation). Reductions in ^{13}C T_1 relaxation values indicated fluorescein could be efficiently encapsulated with the dendrimer and its self-assembly. 2D NOESY

studies further showed fluorescein was encapsulated within the interior of the PPI-3/adipic acid self-assembly.

Red shifts of λ_{max} in UV-vis spectra confirmed that the dyes undergoes changes in solvation upon encapsulation. Reductions in fluorescence emission indicated the dyes were in close contact with the interior amino groups of the dendrimers, enhancing fluorescence quenching. Changes observed in control experiments with ethylenediamine and adipic acid were due to changes in pH, confirming that encapsulation was involved in the dendrimer system.

Chapter 4: Studies of Binding Site Competition in PPI-3/Bimetallic Cation Complexes

Introduction

The presence of multiple functional groups along the periphery and within the interior of dendrimers makes them useful for the chelation of many types of metal cations.[38,39,40,41] These metal/dendrimer complexes can be used in a myriad of applications.

Use as catalysts is one important application of dendrimer/metal complexes. Ford *et al* used PPI complexes of Cu(II), Zn(II), and Co(II) to catalyze the hydrolysis of p-nitrophenyl diphenylphosphate.[42] Rate constants for the reaction were 1.3-6.3 times greater in the presence of PPI-Cu(II) than for PPI alone.

Dendrimers can also be used as metal sequestering agents. Raymond *et al* synthesized salicylate-, catecholate-, and hydroxypyridinomate-functionalized PPI and PAMAM dendrimers,[43] and reported that these dendrimers had a high iron-loading capacity (45 equivalents Fe(II) per dendrimer for salicylate-functionalized PPI). The metal-binding properties of the dendrimers were dependent on the nature of the chelating groups bonded to the dendrimer rather than the size or type of dendrimers. These modified dendrimers may have potential applications in waste water treatment.

Chemical or electrochemical reduction of dendrimer/metal complexes results in the formation of nanoscopic metal particles within the interior of the dendrimers.[38,39,44,45] These dendrimer-encapsulated metal nanoparticles have been used as catalysts.[45,46] Crooks *et al* reported the size-selective hydrogenation of olefins using palladium

nanoparticles encapsulated within PAMAM dendrimers.[47] Size selectivity of the olefins was accomplished by using different generations of the dendrimer. Steric crowding along the surface of the dendrimer increases with an increase in the generation of dendrimers. With lower generations of dendrimer, both linear and branched olefins can access the Pd catalyst to undergo hydrogentation, but with an higher generations of dendrimer, the rate of hydrogenation was greatest for linear olefins.

Dendrimer-encapsulated metal nanoparticles can also be used in imaging applications. Douglas *et al* reported the synthesis of iron oxide/PAMAM dendrimer composites.[48] These nanocomposites resulted in a significant increase in both T_1 and T_2 values of water molecules, making these systems potentially useful as MRI contrast agents.

A better understanding of the interactions between dendrimer and metal cations can help to design more efficient and selective metal sequestering agents or novel catalytic materials. In this study, PPI-3 (Figure 1.3) was used to synthesize a series of dendrimer/bimetallic cation complexes (Cu/Ni, Cu/Co, Cu/Zn, Ni/Co) and then formation of the self-assembly of PPI-3 and decanoic acid was used to extract the dendrimer/metal complexes into organic solvents for purification (Figure 4.1).. UV-vis spectroscopy was used to study the dynamics of the competitive interactions of Cu(II), Ni(II), Co(II), and Zn(II) with PPI-3. In other experiments, the bimetallic complexes of PPI-3 (Cu/Ni/PPI-3 and Cu/Co/PPI-3) were chemically reduced to form PPI-3-encapsulated bimetallic nanoparticles. The quantity of each metal inside the dendrimer/metal complexes and bimetallic nanoparticles was determined semi-quantitatively using energy-dispersive x-ray spectroscopy (EDX).

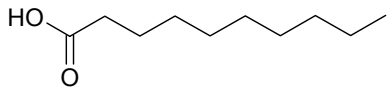

Figure 4.1. The structure of decanoic acid used in this study.

Experimental

General

PPI-3 dendrimer was obtained from Aldrich Chemical Company. $NiCl_2 \bullet 6H_2O$, $ZnCl_2$, and decanoic acid were obtained from Acros Organics, $CuCl_2 \bullet 2H_2O$ and $NaBH_4$ from Fisher Scientific, and $CoCl_2 \bullet 6H_2O$ from J. T. Baker Chemical Company. Dialysis tubing (MWCO = 1000 Da) was obtained from Spectrum Laboratories. All chemicals were used as received without further purification. Concentrations of all reagents used are summarized in Table 4.1.

All EDX spectra were obtained using a JEOL JSM-5310LV scanning electron microscope equipped with an Oxford energy-dispersive x-ray detector. All UV-vis spectra were obtained using a Hewlett-Packard 8452A diode-array spectrophotometer.

Table 4.1. Concentrations of All Reagents Used in This Study.

Reagent	Concentration (M)	
	PPI-3/bimetallic complexes	PPI-3/bimetallic nanoparticles*
$CuCl_2$	0.02007	0.200
$NiCl_2$	0.02008	0.200
$CoCl_2$	0.02005	0.200
$ZnCl_2$	0.02012	----------
decanoic acid**	0.04	----------
PPI-3	0.03067	0.001253

* solutions made in methanol

** solution made in toluene

Table 4.2. Volumes of PPI-3 Solution Used for PPI-3/Bimetallic Cation Complexes.

Molar Ratio (M_1:M_2:PPI-3)	volume PPI-3 (mL)
8:8:0.5	0.5
8:8:1	1
8:8:2	2
8:8:4	4

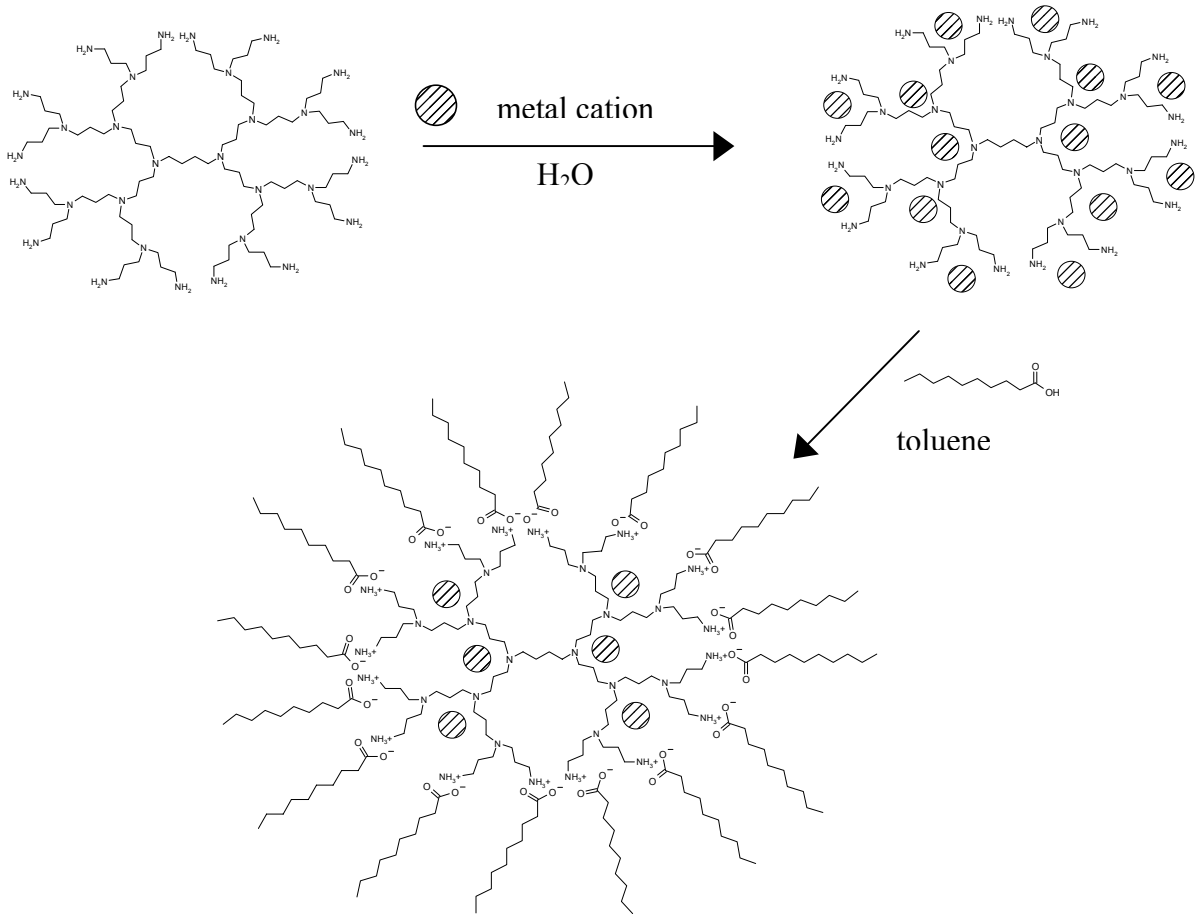

Figure 4.2. Scheme for the formation of PPI-3/bimetallic complexes.

Preparation of PPI-3/bimetallic cation complexes

Aqueous solutions (1 mL) of two metal chlorides were added to a 2 dram sample vial, followed by proportional amounts of PPI-3 solution (Table 4.2). The dendrimer/metal complexes were then extracted using decanoic acid dissolved in toluene (16:1 acid to PPI-3) (Figure 4.2). The mixtures were spun down using a centrifuge to

ensure separation of the toluene and aqueous layers. The lower aqueous layer was removed and discarded. The upper toluene layer was transferred to a clean 2 dram sample vial, and the solvent was evaporated in air yielding pale blue (for Cu/Ni, Cu/Co, and Cu/Zn samples) or colorless (for Ni/Co) solids. The molar ratio of PPI-3 to metal cations was changed to determine the effect of excess binding sites on metal composition of the final product. In other experiments, molar ratio was held constant and decanoic acid extraction was performed at different times to determine the effects of PPI-3 exposure time on metal composition of the final products.

Preparation of PPI-3/bimetallic nanoparticles

Methanolic solutions of the metal chlorides (50.1 μL) were added to a 4-dram sample vial containing 10 mL deionized water. The resulting mixtures were colorless and clear. The vial was capped with a rubber septum and flushed with dry nitrogen gas for approximately 20-30 minutes. A methanolic solution of PPI-3 (0.5 mL) was added to the mixtures, giving light blue reaction mixtures. A 16:1 molar ratio of total metal cations to PPI-3 was maintained to ensure competition between the metal cations for the terminal binding sites of the dendrimer. The reaction mixtures were reduced at different times after addition of PPI-3 using a 5-molar excess of $NaBH_4$ (dissolved in methanol) (Figure 4.3). Upon addition of $NaBH_4$, the reaction mixtures became black, and the reaction mixtures were flushed with nitrogen gas for approximately 30 minutes. The reaction mixture was then purified by dialysis (MWCO = 1000 Da) for 5-6 hours. The resulting solutions were flushed with nitrogen gas to dryness, yielding dark brown to black solids.

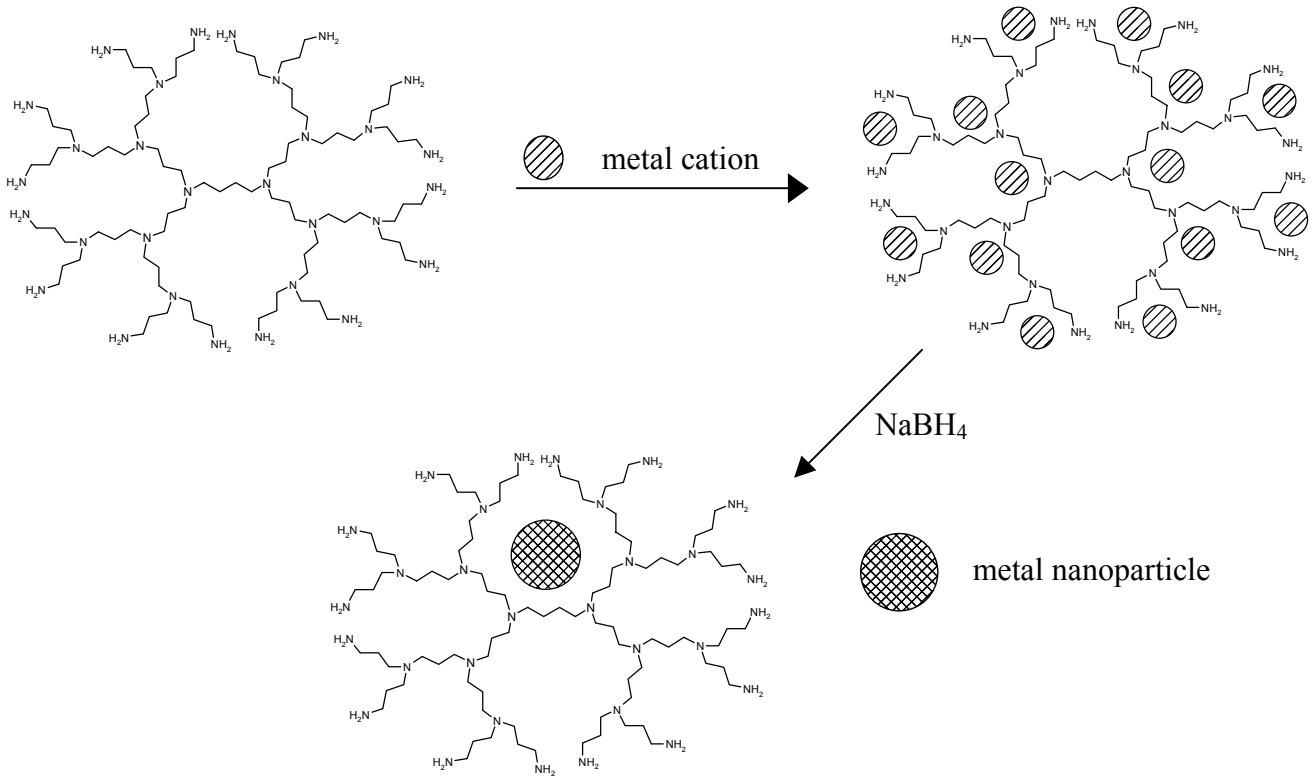

Figure 4.3. Scheme for the formation of PPI-3 encapsulated bimetallic nanoparticles.

Characterization of PPI-3/bimetallic cation complexes and nanoparticles

For UV-vis spectroscopy, all spectra were obtained at 25^{o}C using a Hewlett-Packard 8452A diode-array spectrophotometer equipped with a temperature control bath. 20 μL of an aqueous solution of each metal cation (0.02M) was added to a 1-cm cuvet containing 2 mL deionized water, and a UV-vis spectrum was obtained with water as blank. PPI-3 aqueous solution (0.010 M) was added to the cuvet and a UV-vis spectrum was obtained. For bimetallic cation mixtures, a 16:1 molar ratio of total metal cation to dendrimer was maintained and UV-vis spectra were collected at 1 min intervals over 3 hours to monitor the dynamics of the complexation of metal ions and PPI-3 dendrimer.

For EDX analysis, samples were mounted onto aluminum stubs using double-sided carbon tape. X-ray spectra were collected for 20 minutes real time at 20 kV acceleration voltage, a working distance of 31 mm, and 1500X magnification.

Results and Discussion

For Cu(II), Ni(II), Co(II), or Zn(II) alone in aqueous solutions, the solutions were colorless and clear. For mixtures of Cu(II) with Ni(II), Co(II), or Zn(II), respectively, addition of PPI-3 resulted in a color change to dark blue due to the chelation of Cu(II) with PPI-3. This dark blue color slowly faded over time, suggesting that Cu(II) was slowly being replaced by other metal cations present in the solution.

UV-vis spectroscopy was used to monitor changes in the metal cation/PPI-3 mixtures over time. Cu(II), Ni(II) and Co(II) had λ_{max} values outside the detection limit of the instrument. Complexation with PPI-3 resulted in a broad peak at 268 nm for Cu(II) (Figure 4.4). Changes were also observed for Ni(II), Co(II), and Zn(II) upon

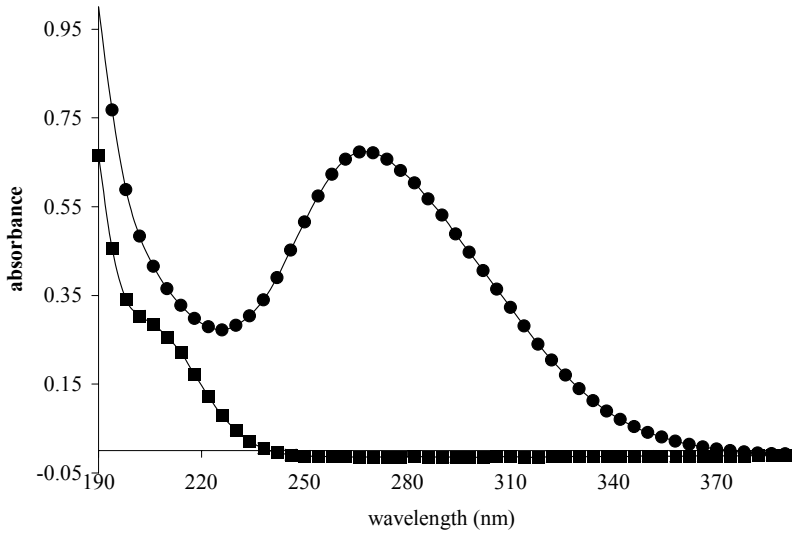

Figure 4.4. UV-vis spectra of Cu(II) in water: (■) alone and (●) with PPI-3.

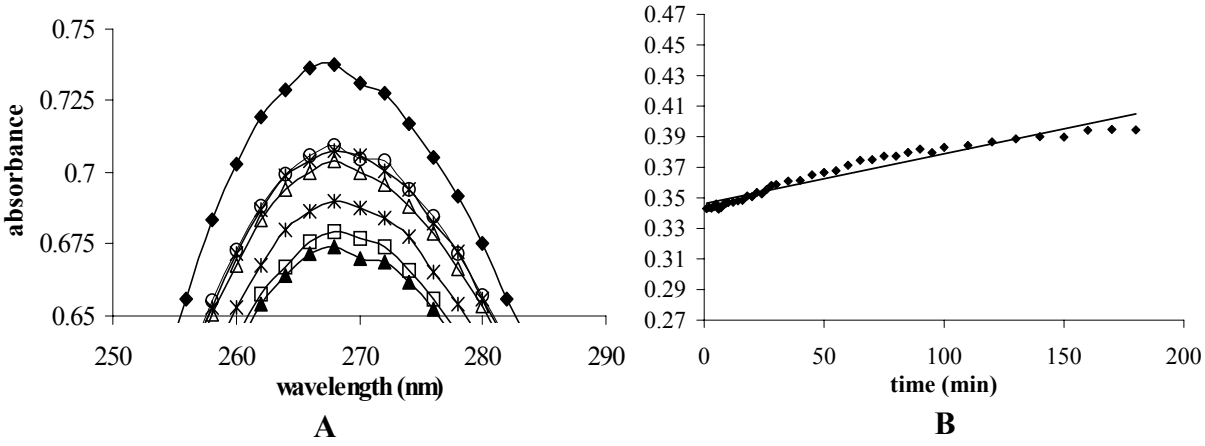

Figure 4.5. (A) UV-vis spectra of cu(II)/Ni(II)/PPI-3 mixture at different times: (◆) 0 min; (○) 1 min; (*) 5 min; (∆) 20 min (●) 60 min; (□) 120 min; (▲) 180 min. (B) Plot of –ln(absorbance$_{268\ nm}$) verses time for Cu(II)/Ni(II)/PPI-3 mixture.

chelation with PPI-3, but λ_{max} values were outside the detection limits of the instrument. When PPI-3 was added to a mixture of Cu(II) and Ni(II) solutions, there was a gradual decrease in absorbance at 268 nm (Figure 4.5A). A plot of absorbance at 268 nm verses time confirmed this decrease (Figure 4.5B). Similar results were observed for Cu(II) and Co(II). These results suggested that Cu(II) and other metal cations compete for the binding sites of the dendrimer.

A closer examination of the dendrimer structure reveals two different types of binding sites: primary amino groups along the periphery of the dendrimer and tertiary amino groups within the interior. These binding sites are expected to have different affinities toward different metal cations because of differences in basicity. Initially, Cu(II) occupies both types of binding sites, likely because the process is kinetically controlled. Cu(II) is then slowly replaced by other metal cations because of the thermodynamic stability of the metal complexes.

PPI-3 self-assembly with long chain monoacids offers a unique method for both binding site isolation and purification of the final product.[24] Protons compete with metal

cations for the primary amino binding sites along the periphery of the dendrimer to form self-assemblies, leaving only the tertiary amino sites within the interior of the dendrimer available for metal binding. These inverse-micelle types of self-assemblies with metal ions chelated inside can be used to extract dendrimer/metal cation complexes from aqueous solutions into organic solvents, such as toluene. Only the PPI-3/metal ion complexes will be soluble in toluene. Thus, purer products can be obtained for further analysis.

X-ray analysis of metal/PPI-3 complexes extracted at different times showed little variation in metal content with time (Table 4.3). For Cu(II)/M_2/PPI-3 bimetallic complexes (where M_2 = Ni(II), Co(II), or Zn(II)), Cu(II) was detected in excess, indicating that it had the greatest affinity toward the interior binding sites of the dendrimer. For Ni/Co/PPI-3 bimetallic complexes, much higher concentrations of Ni were detected.

Table 4.3. Percent Composition of Metal Cation/PPI-3 Complexes Extracted at Different Times Using Decanoic Acid.

Sample	Cu/Co/PPI-3/ decanoic acid		Cu/Ni/PPI-3/ decanoic acid		Cu/Zn/PPI-3/ decanoic acid		Ni/Co/PPI-3/ decanoic acid	
	% Cu	% Co	% Cu	% Ni	% Cu	% Zn	% Ni	% Co
0 min	98.29	1.71	97.19	2.81	99.05	0.95	58.48	41.52
1 min	98.51	1.49	91.18	8.82	93.69	6.31	57.77	42.23
5 min	95.92	4.08	94.51	5.49	97.9	2.1	58.91	41.06
10 min	95.26	4.74	95.23	4.77	97.16	2.84	62.7	37.3
20 min	97.09	2.91	96.76	3.24	97.17	2.83	62.25	37.75
30 min	97.08	2.92	91.64	8.36	96.98	3.02	60.25	39.75
60 min	96.81	3.19	90.32	9.68	96.75	3.25	63.8	36.2
90 min	97.14	2.86	95.52	4.48	96.58	3.42	61.3	38.7

Table 4.4. Percent Composition of Metal Cation/PPI-3 Complexes Using Different Ratios of PPI-3 to Metal Cations Extracted with Decanoic Acid.

Ratio metal:metal:PPI-3	Cu/Ni/PPI-3/ decanoic acid		Cu/Co/PPI-3/ decanoicacid		Cu/Zn/PPI-3/ decanoicacid		Ni/Co/PPI-3/ decanoicacid	
	% Cu	% Ni	% Cu	% Co	% Cu	% Zn	% Ni	% Co
8:8:0.5	99.92	0.08	99.98	0.02	99.41	0.59	59.31	40.69
8:8:1	91.39	8.61	94.28	5.72	67.43	32.57	60.29	39.71
8:8:2	87.93	12.07	91.78	8.22	65.86	34.14	71.22	28.78
8:8:4	64.51	35.49	78.94	21.06	45.72	54.28	92.1	7.9

When less than a stoichiometric amount of PPI-3 was present in Cu/M_2/PPI-3 mixtures, Cu was prevalent complexation (Table 4.4). As the amount of PPI-3 increased, the amount of Cu decreased, with a simultaneous increase in the other metal cation present in the final product. With an increase in PPI-3 concentration, the total number of interior binding sites increases. When all of the Cu(II) cations are chelated by these sites, any other binding sites not occupied by Cu(II) are available for other metal cations in the reaction mixture. Ni/Co/PPI-3 mixtures showed a different trend from the Cu/metal/PPI-3 mixtures, however. As the amount of PPI-3 increased, the amount of Ni increased. These results indicated that the metal binding competition observed in the UV-vis spectroscopy studies must occur at the peripheral binding sites of the dendrimer. When the PPI-3/decanoic acid self-assembly forms, via proton transfer to form ion pairs, the protons can displace the metal cations chelated with the primary amino groups of the dendrimer. Therefore, only metal cations chelated by the interior binding sites are kept intact and carried into the toluene layer.

Hard Lewis acids tend to form complexes in which electrostatic interactions are dominant, while soft Lewis acids form complexes in which covalent bonding is more important. Hard Lewis acids bond in the order: $R_3P << R_3N$, $R_2S << R_2O$, while soft Lewis acids show the opposite trend.[49] Cu(II), being a softer Lewis acid, prefers to bind

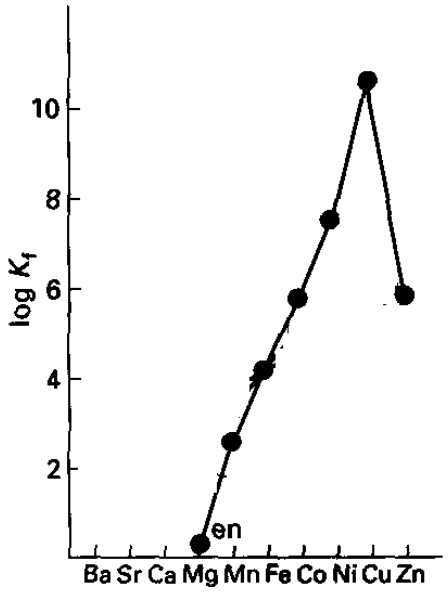

Figure 4.6. Irving-Williams series for ethylenediamine and various metals.[49]

to the nitrogen atoms of the interior tertiary amino groups of the dendrimer. Ni(II), Co(II), and Zn(II), being slightly harder Lewis acids, prefer to bind to the primary amines along the periphery, where they can also chelate with oxygen atoms of water molecules or counterions (Cl^-), which are relatively harder Lewis bases compared to nitrogen.

The trend for Ni(II)/Co(II) bimetallic complexes with PPI-3 (Tables 4.3 and 4.4) can be understood by examining the Irving-Williams series for ethylenediamine (Figure 4.6). In many ways, ethylenediamine is similar to PPI-3: (1) same type of binding sites (amines); (2) ethylenediamine is a bidentate ligand, and PPI-3 is a multidentate ligand. In the Irving-Williams series, binding constants for Ni(II) and Co(II) are similar. When a limited number of binding sites are available, nearly equal amounts of Ni(II) and Co(II) were observed. As the number of binding sites increases, the differences in the binding constants becomes more distinct, and the greater competition between Ni(II) and Co(II) is

observed, resulting in an increase in the amount of Ni(II) with an increase in the amount of PPI-3.

EDX analyses were performed on Cu(0)/Ni(0)/PPI-3 and Cu(0)/Co(0)/PPI-3 bimetallic nanoparticles obtained at different times by chemical reduction with $NaBH_4$. The binding site competition among the metal cations for the primary amino groups of the dendrimer can be gauged by reducing the cations to form zerovalent metal nanoparticles within the interior of the dendrimer at different times after addition of PPI-3. For the Cu/Ni/PPI-3 system, there was an initial 59.36% Cu and 40.64% Ni. There was a reduction in %Cu and a simultaneous increase in %Ni from 0 minutes to 5 minutes. From 10 to 20 minutes, there was slight oscillation in the trend, but, in general, there was an increase in % Cu and a decrease in % Ni. At 60 minutes, the initial trend was followed, and more Ni was present than Cu in the sample (51.68% and 48.32%, respectively) (Figure 4.7).

A similar trend was observed for Cu/Co bimetallic nanoparticles (Figure 4.8). However, there was a greater difference observed in the relative amounts of Cu and Co than that for Cu and Ni. Initial percentages of Cu and Co were 69.06% and 30.94%, respectively. After 60 minutes, there was 46.48% Cu and 65.52% Co in the sample. These results further confirmed that the competition of metal cations for the binding sites of PPI-3 occurs on the periphery of the dendrimer.

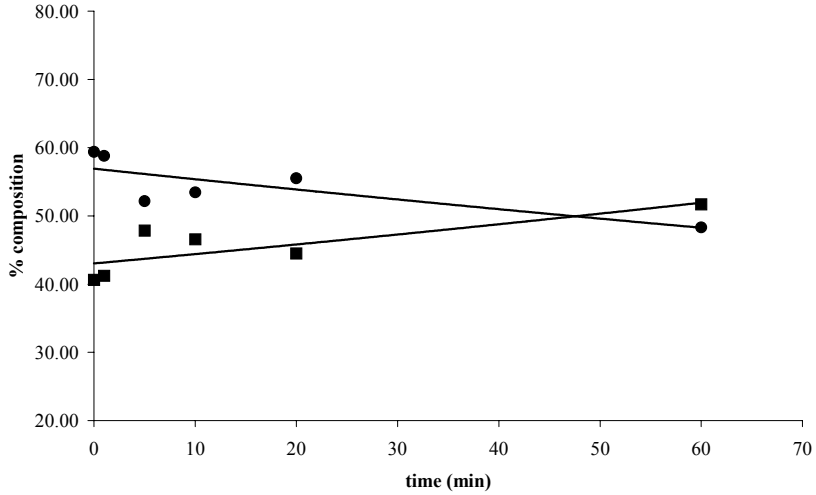

Figure 4.7. Comparison of %Cu (●) and % Ni (■)in Cu/Ni/PPI-3 bimetallic nanoparticles formed by reduction using $NaBH_4$ at different times.

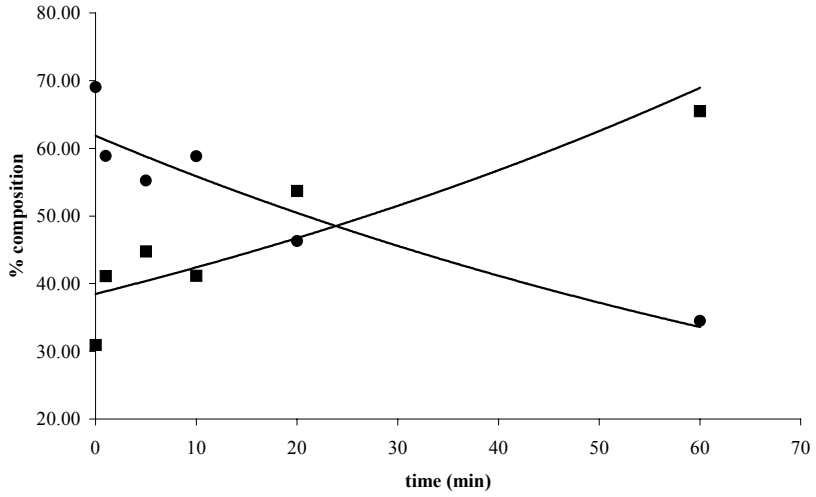

Figure 4.8. Comparison of %Cu (●) and % Co (■)in Cu/Co/PPI-3 bimetallic nanoparticles formed by reduction using $NaBH_4$ at different times.

Conclusions

PPI-3 can effectively chelate Cu(II), Ni(II), Co(II), and Zn(II) cations in aqueous solutions. UV-vis spectroscopy suggests that competition between Cu(II) and the other metal cations occurs due to differences in the stability of the PPI-3/metal cation complexes. EDX studies on the equal molar bimetallic ion complexes with PPI-3 with

the extraction using decanoic acid in toluene implied that the metal binding competition occurs on the periphery (primary amino groups) of the dendrimer. EDX analyses of the dendrimer/bimetallic nanoparticles showed a decrease in % Cu and a simultaneous increase in % Ni or % Co over time, further indicating the metal competition for the periphery binding sites of the dendrimer. These differences in ability to chelate metals make PPI dendrimers interesting materials for selectively sequestering different metals and as templates for the production of novel nanomaterials.

Chapter 5: Studies of the Catalytic Properties of PPI Dendrimers.

Introduction

One important property of dendrimers is catalysis.[14,15,16] Dendrimers catalysts have many of the advantages of both homogeneous catalysts (solubility, high reaction rates) and heterogeneous catalysts (ease in separation).[50] They have been used to catalyze a variety of reactions[15]

Catalytic sites can be located at the core of dendrimers. Suslick *et al* synthesized a series of dendrimer metalloporphyrins based on poly(phenylester) dendritic arms to a [Mn(TPP)(Cl)] core (5,10,15,20-tetrakis(3',5'-hydroxyphenyl)-porphinatomanganese(III) chloride) to give a sterically protected metal center.[51] These dendrimers were tested for catalyzing the epoxidation of olefins, and showed much greater selectivity for the less-sterically hindered double bond of dienes compared to simple Mn(TPP)(Cl).

Catalytic sites of dendrimers can also be located within the interior of the dendrimer. Crooks *et al* reported the synthesis of palladium nanoparticles trapped within the interiors of different generations of PAMAM dendrimers and used them as catalysts for the hydrogenation of olefins.[47] These PAMAM-encapsulated Pd nanoparticles showed greater selectivity for hydrogenation of linear olefins with an increase in dendrimer generation due to an increase in steric hindrance along the periphery of the dendrimer.

Dendrimers can also host catalytic sites along the periphery of the of their structures. Schwickardi *et al* synthesized a dendritic diphosphine by double

phosphinomethylation of the primary amino ends of PPI-3 dendrimer.[52] The resulting dendrimer contains 16 bidentate ligands, and can chelate a variety of transition metals. Pd-complexed dendrimer was utilized as a catalyst for the Heck reaction of bromobenzene and styrene to form stillbene. This dendritic catalyst showed significantly higher activity in comparison with non-dendritic Pd complexes due to the higher thermal stability of the dendritic complexes.

While investigating the encapsulation of fluorescent dyes within PPI/diacid acid self-assemblies (see Chapter 3), it was discovered that PPI dendrimers catalyzed the hydrolysis of the $DEBF_4$ dye (a diester) to $DABF_4$ (a diacid) (Figure 5.1). In this study, the catalytic properties of PPI-3 (Figure 1.3) were investigated further using UV-vis and NMR spectroscopies.

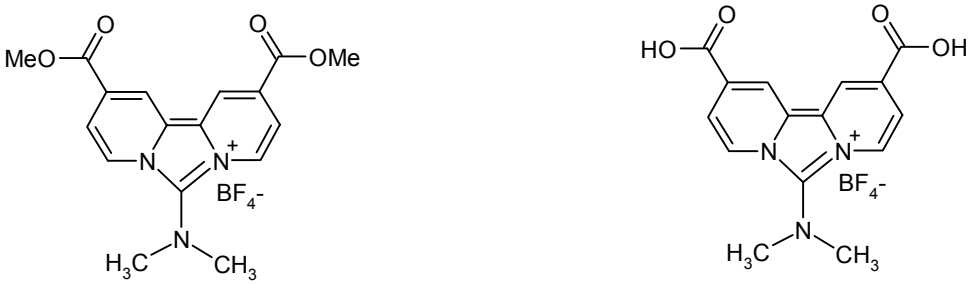

A **B**

Figure 5.1. Structures of fluorescent dyes: (A) $DEBF_4$; (B) $DABF_4$.

Experimental

Chemicals

$DEBF_4$ and $DABF_4$ dyes were provided by Dr. Robert Morgan of Marshall University. PPI-3 was obtained from Aldrich Chemical Company. Deuterium oxide was

purchased from Norrell, Inc and DMSO-d_6 was purchased from Cambridge Isotope Laboratories.

UV-vis spectroscopy

All UV-vis spectra were obtained at 28°C using a Hewlett-Packard 8452A diode-array spectrophotometer equipped with a temperature control device. The stock solutions of all reagents were prepared in deionized water: PPI-3 (.009817 M); $DEBF_4$ (0.00231 M); $DABF_4$ (0.000207 M). A certain volume of PPI-3 solution (Table 5.1) and 2 mL deionized water were added to a 1-cm quartz cuvet, and the resulting solution was used as a blank for UV-vis measurerments. 20 μL of $DEBF_4$ solution was then added to the cuvet, and UV-vis spectra were obtained for different molar ratios of PPI-3 and $DEBF_4$ (Table 5.1). Comparison studies were performed between the $DEBF_4$/PPI-3 mixtures and $DABF_4$.

Table 5.1 $DEBF_4$ and PPI-3 Concentrtion Used in UV-vis Studies.

[PPI-3]:[$DEBF_4$]	volume $DEBF_4$ solution (μL)	volume PPI-3 solution (μL)	[$DEBF_4$] (M)	[PPI-3] (M)
0.25:1	20	1.18	$2.31x10^{-5}$	$5.792x10^{-5}$
0.5:1	20	2.36	$2.31x10^{-5}$	$1.158x10^{-5}$
1:1	20	4.71	$2.31x10^{-5}$	$2.312x10^{-5}$
2:1	20	9.42	$2.31x10^{-5}$	$4.624x10^{-5}$
4:1	20	18.8	$2.31x10^{-5}$	$9.228•x10^{-5}$
8:1	20	37.7	$2.31x10^{-5}$	$18.51x10^{-5}$
16:1	20	75.4	$2.31x10^{-5}$	$37.01x10^{-5}$

NMR spectroscopy

$DEBF_4$ was dissolved in 0.266 mL of DMSO-d_6 in a 5 mm NMR tube, and PPI-3 was dissolved in 0.434 mL of D_2O in a conical vial. The PPI-3 solution was then

Table 5.2. $DEBF_4$ and PPI-3 Concentrations Used in NMR Studies.

Molar Ratio PPI-3 to $DEBF_4$	mass $DEBF_4$ (g)	mass PPI-3 (g)	[$DEBF_4$] (M)	[PPI-3] (M)
025:1	0.0049	0.005	0.01686	0.00423
0.5:1	0.0049	0.01	0.01686	0.00847
0.75:1	0.005	0.0153	0.01721	0.01296
1:1	0.005	0.0202	0.01721	0.01711

transferred to the NMR tube. ^{1}H NMR spectra were collected at 5 min intervals over various time periods (depending on the amount of PPI-3). Concentrations of all reagents are summarized in Table 5.2. A comparison study was performed using $DABF_4$ (0.005 g) and PPI-3 (0.0434 g) dissolved in 0.7 mL of mixed DMSO-d_6/D_2O (0266 mL/0.434 mL) in a 5 mm NMR tube. Kinetic experiments were performed holding $DEBF_4$ concentration constant and changing PPI-3 concentration to determine the effect of PPI-3 concentration on the rate of hydrolysis. All NMR spectra were acquired at ambient temperature on a Varian UnityPlus 500 MHz spectrometer equipped with a Nalorac PFG triple resonance ^{1}H/^{13}C/X probe (X tunable from ^{15}N to ^{31}P) and a Varian broadband probe. All NMR data were processed using Varian VNMR software on a Sun UltraSPARC-60 workstation.

^{1}H NMR spectra were acquired at 499.220 MHz using a 5146.0 Hz spectral window, 3.0 μs (60^o) pulse width, 3 s acquisition time, and 1 transient. Spectra were collected over various time periods with a preacquisition delay of 300 seconds. ^{13}C NMR spectra were acquired at 125.541 MHz using a 1.0 s acquisition time, 27008.8 Hz spectral window, 8.2 μs (90^o) pulse width, 10 s relaxation delay, and 4096 transients with WALTZ-16 modulated ^{1}H decoupling.

Results and Discussion

Confirmation of Hydrolysis

Initially, studies of $DEBF_4$ were concerned with the encapsulation of this dye within PPI/diacid self-assemblies. λ_{max} in UV-vis spectra of the dye blue-shifted in the presence of PPI-3 (Figure 5.2), and the intensity of the methoxy resonance of $DEBF_4$ in the ^1H NMR spectra decreased over time with a simultaneous increase in the intensity of the methoxy resonance of methanol (Figure 5.3). These results suggested that the diester form of the dye , $DEBF_4$, was hydrolyzed to the diacid form of the dye, $DABF_4$.

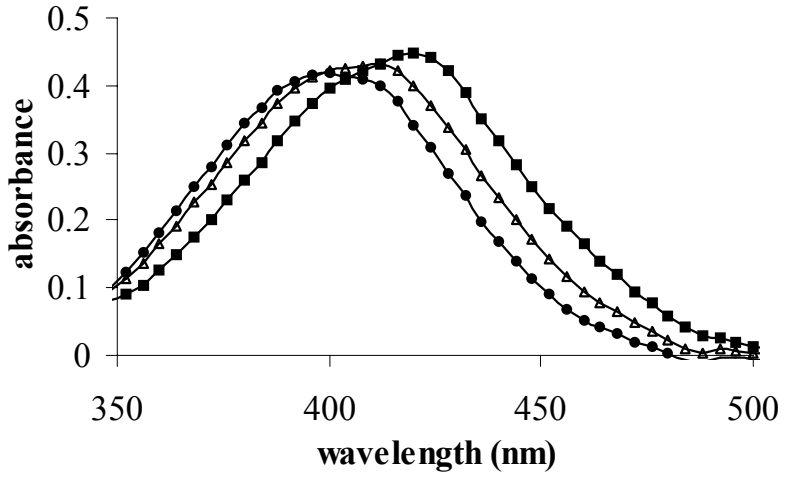

Figure 5.2. UV-vis spectra of $DEBF_4$ in presence of PPI-3 (1:2 molar ratio): (■) 0 min; (△) 60 min; (●) 240 min.

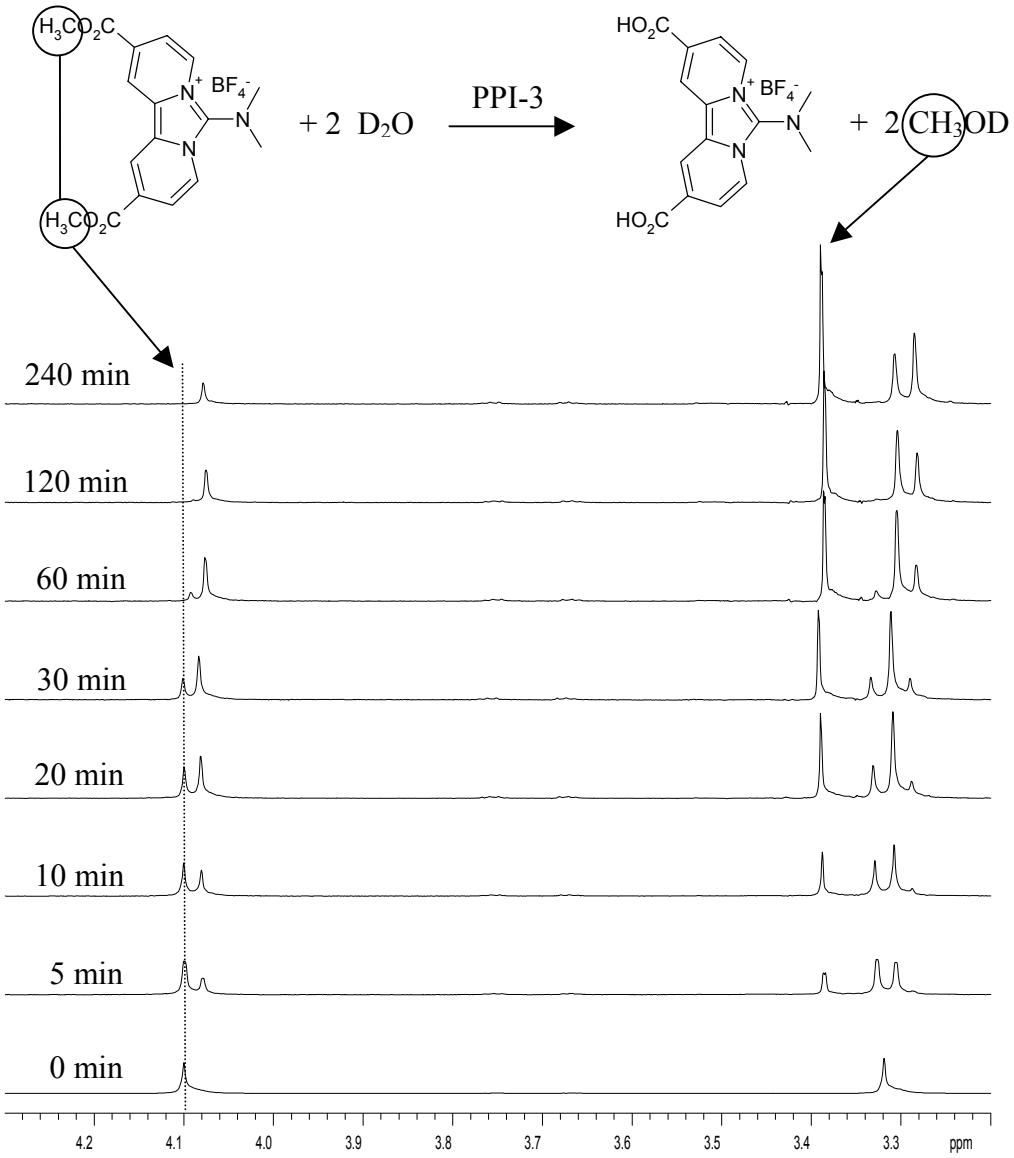

Figure 5.3. Expansion of ^{1}H NMR spectra of $DEBF_4$ (aliphatic region) in the presence of PPI-3 (1:1 molar ratio) at different times.

A comparison of the UV-vis spectra of $DABF_4$ and $DEBF_4$ (with PPI-3) after reaction showed that the profiles of the UV-vis absorption were quite similar. Fitting the $DEBF_4$ with a certain coefficient (1.4) to the $DABF_4$ spectrum, the subsequent spectral

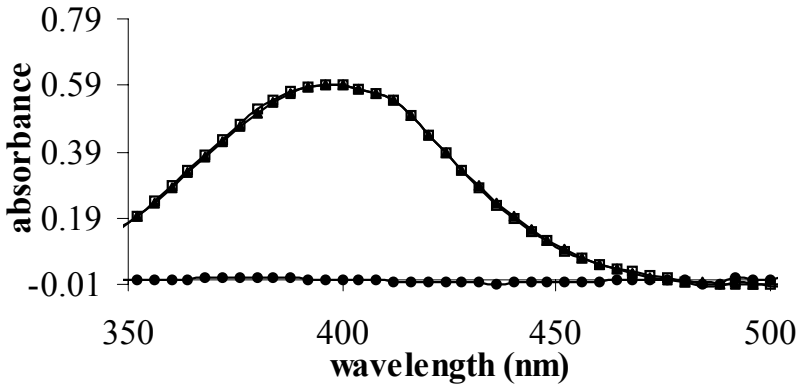

Figure 5.4. UV-vis spectra of: (□) $DABF_4$ in water; (▲) $DEBF_4$ with PPI-3 in water after 240 min fitted with a coefficient (1.4) to the $DABF_4$ spectrum; (●) spectral subtraction.

subtraction showed that the two spectra had the same profile, suggesting that $DEBF_4$ in aqueous solutions was hydrolyzed to form $DABF_4$ (Figure 5.4).

Because $DEBF_4$ and $DABF_4$ differ only in functionality at the carbonyl group, a comparison of these carbonyl resonances in ^{13}C NMR spectra can be used to confirm the hydrolysis of $DEBF_4$. The ^{13}C carbonyl resonance of $DEBF_4$ mixed with PPI-3 after ~1 week closely matched the carbonyl resonance of $DABF_4$ with PPI-3, compared with $DEBF_4$ alone (Figure 5.5). This information further proved the hydrolysis of $DEBF_4$ to $DABF_4$.

Once the hydrolysis of $DEBF_4$ in the presence of PPI-3 was confirmed, it was important to establish PPI-3 acts as a catalyst and not a substrate (reactant) in the reaction. No changes were observed in the ^1H NMR resonances of PPI-3 mixed with $DEBF_4$ over various periods of time (Figure 5.6). This indicated that PPI-3 does not undergo any permanent chemical change in the course of hydrolysis, which shows PPI-3 acts as a catalyst in the reaction.

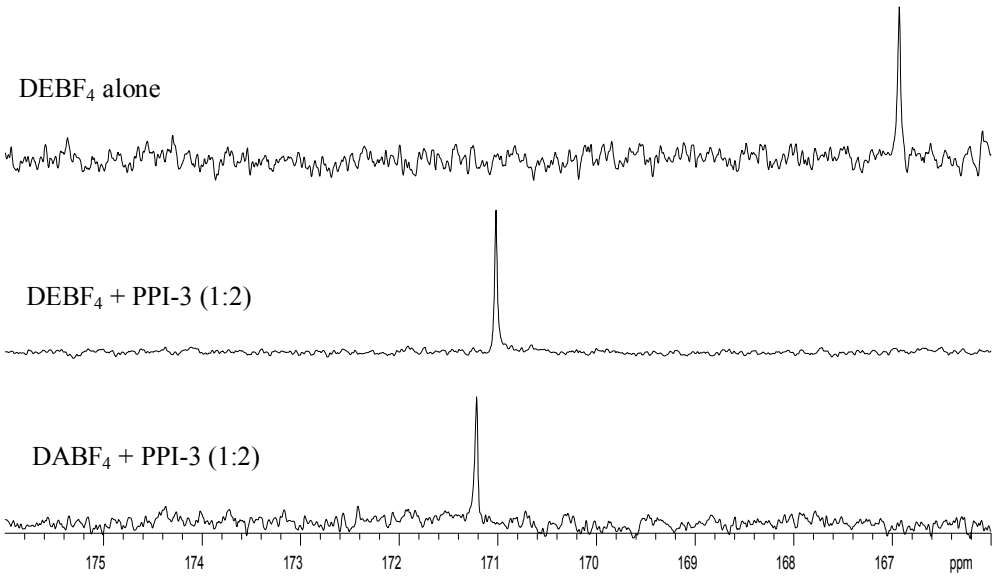

Figure 5.5. Expansion of ^{13}C NMR spectra (carbonyl region) of $DEBF_4$ and $DABF_4$ in D_2O/DMSO-d_6.

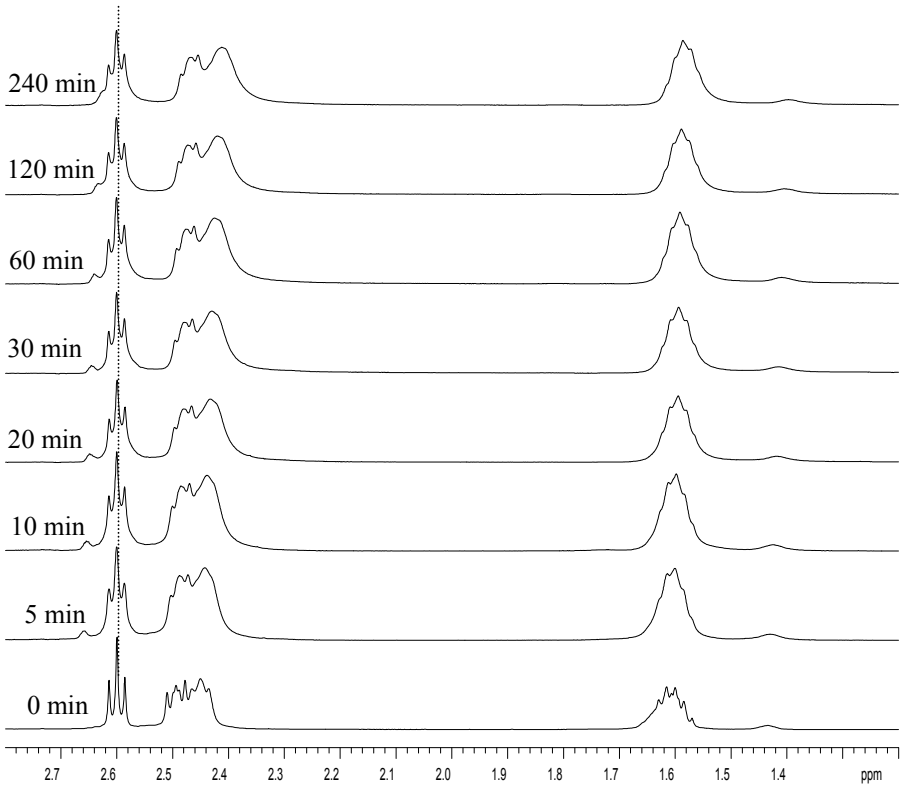

Figure 5.6. ^1H NMR spectra of PPI-3 with $DEBF_4$ at different times (1:1 molar ratio PPI-3 to $DEBF_4$).

Generally, hydrolysis of $DEBF_4$ follows first order rate kinetics based on the following rate equation:

$$\begin{aligned} rate &= k_{cat} \times [DEBF_4] \\ k_{cat} &= k \times [PPI-3] \times [H_2O] \end{aligned} \quad \textbf{(1)}$$

where k is the intrinsic reaction rate constant and k_{cat} is the PPI-3 catalyzed reaction rate constant; [DEBF4], [PPI-3], and [H_2O] are concentrations of $DEBF_4$, PPI-3, and H_2O, respectively. Because H_2O is present in great excess in the reaction mixtures, and PPI-3 is a catalyst, the rate equation can be simplified to

$$rate = k_{obs} \times [DEBF_4] \quad \textbf{(2)}$$

where k_{obs} is the pseudo first-order rate constant, and can be expressed as

$$k_{obs} = k \times [PPI\text{-}3] \times [H_2O] \quad \textbf{(3)}$$

Since a catalyst can change a raction rate constant, plotting the pseudo first-order rate constants verses the concentration of PPI-3 results in a linear plot, where the slope of the line is the PPI-3 catalyzed reaction rate constant, k_{obs2}, and

$$k_{obs2} = k \times [H_2O] \quad \textbf{(4)}$$

Rearranging the above equation to solve for k yields the intrinsic reaction rate constant for the hydrolysis.

UV-vis studies

In the UV-vis spectra, $DEBF_4$ and $DABF_4$ have a λ_{max} at 420 nm and 400 nm, respectively. To calculate concentrations of $DEBF_4$ during hydrolysis, the following equations were used:

$$A_{400} = \varepsilon_{DEBF_4(400)} \times [DEBF_4] + \varepsilon_{DABF_4(400)} \times [DABF_4] \qquad \textbf{(5)}$$

$$A_{420} = \varepsilon_{DEBF_4(420)} \times [DEBF_4] + \varepsilon_{DABF_4(420)} \times [DABF_4] \qquad \textbf{(6)}$$

where A_{400} and A_{420} were the absorbances at 400 nm and 420 nm, respectively, [$DABF_4$] and [$DEBF_4$] are the concentrations of $DABF_4$ and $DEBF_4$ at different times, respectively, and ε_{400} and ε_{420} are the molar absorptivity constants of $DABF_4$ and $DEBF_4$, respectively. A plot of the negative of the natural log of [$DEBF_4$] verses time yields linear plots, where the slope of the line is the pseudo first-order rate constant (Figure 5.7). Pseudo first-order rate constants for all experiments are summarized in Table 5.3. A plot of the pseudo first-order rate constants verses concentration of PPI-3 gives in a linear plot, where the slope of the line is the second-order rate constant (215.34 $mol^{-1} \bullet L \bullet min^{-1}$)

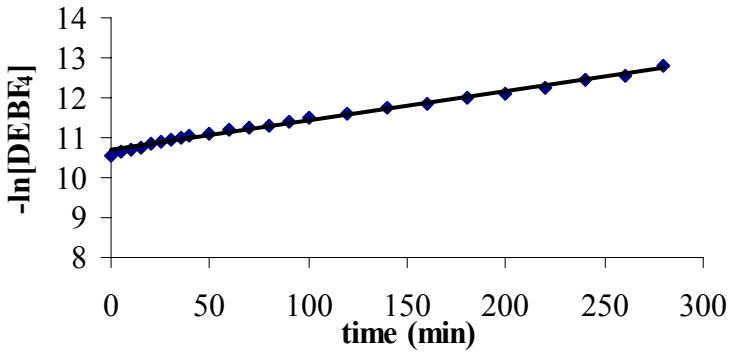

Figure 5.7. Plot of –ln[$DEBF_4$] verses time for PPI-3 catalyzed hydrolysis of $DEBF_4$ for the UV-vis study (2:1 molar ratio PPI-3 to $DEBF_4$).

Table 5.3. Pseudo First-Order Rate Constants for UV-vis Study.

Molar Ratio PPI-3 to $DEBF_4$	$[DEBF_4]$ (M)	[PPI-3] (M)	Pseudo first-order rate constant (min^{-1})
0.25:1	$2.31 \cdot 10^{-5}$	$5.792 \cdot 10^{-5}$	3.197×10^{-4}
0.5:1	$2.31 \cdot 10^{-5}$	$1.158 \cdot 10^{-5}$	13.36×10^{-4}
1:1	$2.31 \cdot 10^{-5}$	$2.312 \cdot 10^{-5}$	21.68×10^{-4}
2:1	$2.31 \cdot 10^{-5}$	$4.624 \cdot 10^{-5}$	84.69×10^{-4}
4:1	$2.31 \cdot 10^{-5}$	$9.228 \cdot 10^{-5}$	204.5×10^{-4}
8:1	$2.31 \cdot 10^{-5}$	$18.51 \cdot 10^{-5}$	349.5×10^{-4}
16:1	$2.31 \cdot 10^{-5}$	$37.01 \cdot 10^{-5}$	787.3×10^{-4}

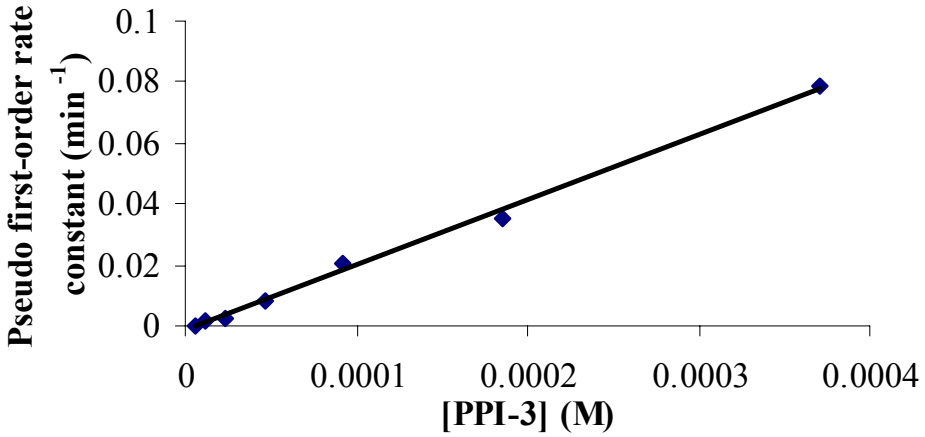

Figure 5.8. Plot of pseudo first-order rate constants verses [PPI-3] for UV-vis study.

(Figure 5.8). The PPI-3 catalyzed reaction rate constant was calculated using equation (4):

$$k = \frac{k_{obs2}}{[H_2O]} = 3.876 \text{ mol}^{-2} \cdot L^2 \cdot min^{-1}$$

A careful examination of the structure of $DEBF_4$ shows that the dye has two equivalent ester groups. Each ester group would have an equal probability to undergo hydrolysis, therefore, one would expect a sequential hydrolysis of the ester groups. A

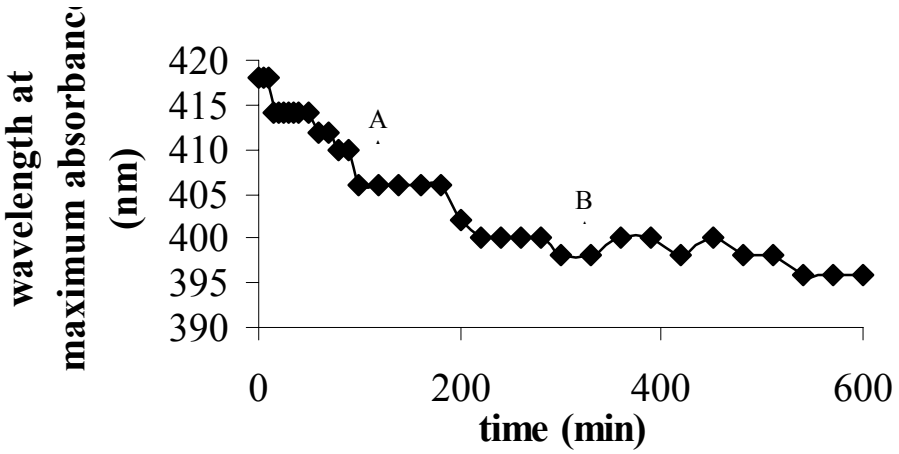

Figure 5.9. Plot of wavelength at maximum absorbance verses time for PPI-catalyzed hydrolysis of $DEBF_4$ (2:1 molar ratio PPI-3 to $DEBF_4$).

plot of the λ_{max} verses time (Figure 5.9) shows that the ester groups of $DEBF_4$ indeed react sequentially. Region A results from the hydrolysis of one of the ester functionalities to the acid, leaving the other ester group unreacted. Region B is a result of hydrolysis of the other ester group to yield $DABF_4$.

NMR studies

For NMR studies, the real-time concentrations of DEBF can be calculated using the following equation:

$$\left[DEBF_4\right] = \left[DEBF\right]_0 \cdot \frac{I_{MeO}}{I_{aromatics}} \times \frac{48.41}{51.59} \qquad \textbf{(7)}$$

where $[DEBF_4]$ and $[DEBF_4]_0$ are the real time and initial concentrations of $DEBF_4$, respectively, $I_{aromatics}$ and I_{MeO} are the values of integration of the aromatic and methoxy

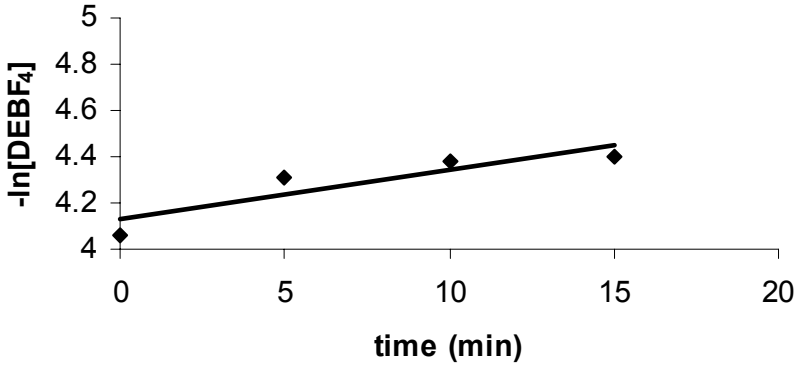

Figure 5.10. Plot of –ln[$DEBF_4$] verses time for PPI-3 catalyzed hydrolysis of $DEBF_4$ for the NMR study (0.5:1 molar ratio PPI-3 to $DEBF_4$.

Table 5.4. Pseudo First-Order Rate Constants for NMR study.

Molar Ratio PPI-3 to $DEBF_4$	[PPI-3] (10^{-3} M)	[$DEBF_4$] (10^{-3} M)	pseudo first-order rate constant (10^{-3} min^{-1})
0.25:1	4.234	17.21	17.49
0.5:1	8.469	16.86	21.4
0.75:1	12.76	17.21	37.77
1:1	17.11	17.21	53.00

regions of $DEBF_4$, and 48.41/51.59 is the ratio of aromatic integration to methoxy integration of $DEBF_4$ before reaction. A plot of the negative of the natural log [$DEBF_4$] verses time yields linear plots, where the slope of the plot is the pseudo first-order rate constant (Figure 5.10). Pseudo first-order rate constants for all experiments are summarized in Table 5.4. A plot of the pseudo first-order rate constants verses concentration of PPI-3 gives the PPI-3-catalyzed reaction rate constant (2.867 $mol^{-1} \bullet L \bullet min^{-1}$) (Figure 5.11) and the real time rate constant was

$$k = \frac{k_{obs2}}{[D_2O]} = 0.09248 \text{ mol}^{-1} \cdot L^2 \cdot min^{-1}$$

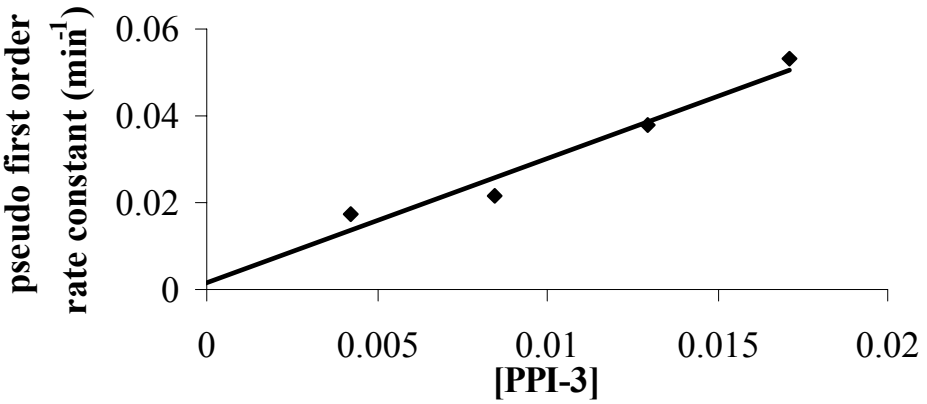

Figure 5.11. Plot of pseudo first-order reate constants verses [PPI-3] for NMR study.

The PPI-3-catalyzed reaction rate constant obtained from the UV-vis studies was approximately 75X greater than the reaction rate constant from the NMR studies. These results were likely due to the high concentration of reagents in the NMR studies compared to the UV-vis studies. This high concentration of reagents would make diffusion of the dye molecules to and from the PPI-3 molecules difficult, reducing the rate of hydrolysis. Viscosity of the reaction mixtures in the NMR studies, due to the high concentration of PPI-3, would also make diffusion difficult, reducing the rate of hydrolysis.

Mechanism of Reaction

UV-vis studies of the hydrolysis of $DEBF_4$ in the presence of PPI-3 show that the reaction is sequential, with one ester being hydrolyzed at a time (Figure 5.9). These results suggest that the interactions of PPI-3 with $DEBF_4$ may orient the dye molecule so that it is in a favorable position to undergo hydrolysis. Once hydrolysis of one ester

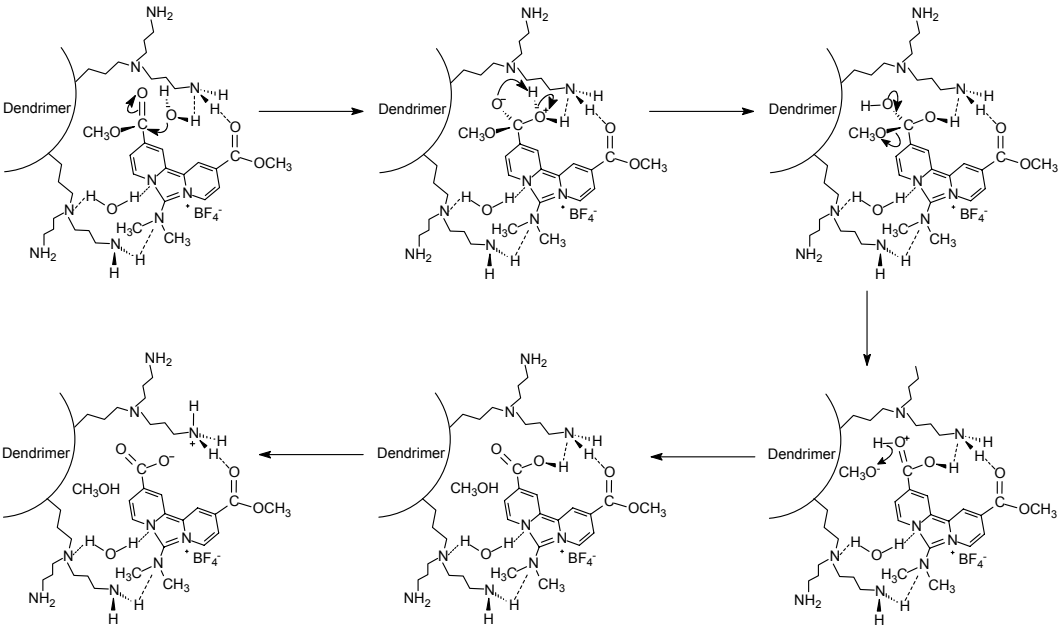

Figure 5.12. Potential mechanism for the PPI-catalyzed hydrolysis of $DEBF_4$.

functionality occurs, the dye diffuses away from the dendrimer and leaves the other ester available for hydrolysis (Figure 5.12).

Conclusions

The catalytic properties of PPI dendrimers for the hydrolysis of esters was investigated using UV-vis and NMR spectroscopies. PPI-3 catalyzes this reaction at room temperature and under mild pH conditions. Rates of reaction determined from the UV-vis studies were approximately 75X greater than the rates determined from the NMR studies due to lower concentrations of reagents and lower viscosity of the reaction mixtures in the UV-vis studies compared to the NMR studies. The dendrimer may act as a reaction vessel to orient the ester for optimal positions for hydrolysis reactions. This mechanism is being investigated.

References

1. Tomalia, D. A.; Naylor, A. M.; Goddard III, W. A. *Angew. Chem. Int. Ed. Engl.* **1990**, 29, 138-175.
2. Fréchet, J. M. J. and Tomalia, D. A. Dendrimers and Other Dendritic Polymers. New York: John Wiley and Sons. 2001.
3. Buhleier, E.; Wehner, W.; Vögtle, F. *Synthesis*. **1978**, 155-158.
4. Wörner, C. and Mülhaupt, R. *Angew. Chem. Int. Ed. Engl.* **1993**, 32(9), 1306-1308.
5. de Brabander-van den Berg, E. M. M. and Meijer, E. W. *Angew. Chem. Int. Ed. Engl.* **1993**, 32(9), 1308-1311.
6. Hawker, C. and Fréchet, J. M. J. *J. Chem. Soc., Chem. Commun.* **1990**, 1010-1013.
7. Hawker, C. J. and Fréchet, J. M. J. *J. Am. Chem. Soc.* **1990**, 112(21), 7638-7647.
8. Fréchet, J. M. J. *Science* **1994**, 263, 1710-1715.
9. Bosman, A. W.; Janssen, H. M.; Meijer, E. W. *Chem. Rev.* **1999**, 99(7), 1665-1688.
10. Jansen, J. F. G. A.; de Brabander-van den Berg, E. M. M.; Meijer, E. W. *Science*, **1994**, 266, 1226-1229.
11. Liu, M.; Kono, K.; Fréchet, J. M. J. *J. Control. Release.* **2000**, 65, 121-131.
12. Baars, M. W. P. L.; Froehling, P. E.; Meijer, E. W. *Chem. Commun.* **1997**, 1959-1960.
13. Zanini, D. and Roy, R. *J. Am. Chem. Soc.* **1997**, 119(9), 2088-2095.
14. Kreiter, R.; Kleij, A. W.; Gebbink, R. J. M. K.; van Koten, G. *Top. Curr. Chem.* **2001**, 217, 164-199.
15. Astruc, D. and Chardac, F. *Chem. Rev.* **2001**, 101(9), 2991-3023.
16. Twymann, L. J.; King, A. S. H.; Martin, I. K. *Chem. Soc. Rev.* **2002**, 31, 69-82.
17. Voet, D.; Voet, J. G.; Pratt, C. W. *Fundamentals of Biochemistry*. New York: John Wiley and Sons, Inc. 1999.
18. Philp, D. and Stoddart, J. F. *Angew. Chem. Int. Ed. Engl.* **1996**, 35, 1154-1196.
19. Jolliffe, K. A.; Timmerman, P.; Reinhoudt, D. N. *Angew. Chem. Int. Ed.* **1999**, 38(7), 933-937.
20. Klok, H. A.; Jolliffe, K. A.; Schauer, C. L.; Prins, L. J.; Spatz, J. P.; Möller, P. T.; Reinhoudt, D. N. *J. Am. Chem. Soc.* **1999**, 121(30), 7154-7155.
21. Whitesides, G. M.; Simanek, E. E.; Mathias, J. P.; Seto, C. T.; Chin, D. N. Mammen, M.; Gordon, D. M. *Acc. Chem. Res.* **1995**, 28(1), 37-44.
22. Zeng, F. and Zimmerman, S. C. *Chem. Rev.* **1997**, 97(5), 1681-1712.

23. Baars, M. W. P. L.; Karlsson, A. J.; Sorokin, V.; de Waal, B. F. W.; Meijer, E. W. *Angew. Chem. Int. Ed.* **2000**, 39(23), 4262-4265.

24. Chechik, V.; Zhao, M.; Crooks, R. M. *J. Am. Chem. Soc.* **1999**, 121(20), 4910-4911.

25. Sanders, J. K. M. and Hunter, B. K. *Modern NMR Spectroscopy: A Guide for Chemists*, 2nd Ed. New York: Oxford University Press. 1993.

26. Steed, J. W. and Atwood, J. L. *Supramolecular Chemistry*, New York: John Wiley and Sons, Ltd. 2000.

27. Chai, M.; Niu, Y.; Youngs, W. J.; Rinaldi, P. L. *J. Am. Chem. Soc.* **2001**, 123(20), 4670-4678.

28. Kojima, C.; Kono, K.; Maruyama, K.; Takagishi, T. *Bioconjugate Chem.* **2000**, 11(6), 910-917.

29. Schenning, A. P. H. J.; Peeters, E.; Meijer, E. W. *J. Am. Chem. Soc.* **2000**, 122(18), 4489-4495.

30. Hawker, C. J.; Wooley, K. L.; Fréchet, J. M. J. *J. Chem. Soc., Perkin Trans.* **1993**, 1287-1297.

31. Newkome, G. R.; Moorefield, C. N.; Baker, G. R.; Saunders, M. J.; Grossman, S. H. *Angew. Chem. Int. Ed. Engl.* **1991**, 30(9), 1178-1180.

32. Baars, M. W. P. L.; Froehling, P. E.; Meijer, E. W. *Chem. Commun.* **1997**, 1959-1960.

33. Newhaus, D. and Williamson, M. P. *The Nuclear Overhauser Effect in Structure and Conformational Analysis*. 2nd Ed. New York, Wiley-VCH, Inc. 2000.

34. Sjöback, R.; Nygren, J.; Kubista, M. *Spectrocchimica Acta Part A*. **1995**, 51, L7-L21.

35. Diehl, H. and Horchak-Morris, N. Studies of Fluorescein. V. *Talanta.* **1987**, 34(8), 739-741.

36. UV-vis Absorption Spectroscopy – Theory. http://www.shu.ac.uk/schools/sci/chem /tutorials/molspec/uvvisab1.htm (8 July 2003).

37. Lakowicz, Joseph R. *Principles of Fluorescence Spectroscopy*. 2nd Ed. New York: Kluwer Academic/Plenum Publishers. 1999.

38. Zhao, M.; Sun, L.; Crooks, R. M. *J. Am. Chem. Soc.* **1998**, 120(19), 4877-4878.

39. Zhao, M. and Crooks, R. M. *Chem. Mater.* **1999**, 11(11), 3379-3385.

40. Ottaviani, M. F.; Montalti, F.; Turro, N. J.; Tomalia, D. A. *J. Phys. Chem. B.* **1997**, 101(2), 158-166.

41. Ottaviani, M. F.; Montalti, F.; Romanelli, M.; Turro, N. J.; Tomalia, D. A. *J. Phys. Chem.* **1996**, 100(26), 11033-11042.

42. Vassilev, K. and Ford, W. T. *J. Polym. Sci. Part A.* **1999**, 37, 2727-2736.

43. Cohen, S. M.; Petoud, S.; Raymond, K. N. *Chem. Eur. J.* **2001**, 7(1), 272-279.

44. Balogh, L. and Tomalia, D. A. *J. Am. Chem. Soc.* **1998**, 120(29), 7355-7356.

45. Crooks, R. M.; Zhao, M.; Sun, L.; Chechik, V.; Yeung, L. K. *Acc. Chem. Res.* **2001**, 34(3), 181-190.

46. Crooks, R. M.; Lemon III, B. I.; Sun, L.; Yeung, L. K.; Zhao, M. *Top. Curr. Chem.* **2001**, 212, 82-134.

47. Niu, Y.; Yeung, L. K.; Crooks, R. M. *J. Am. Chem. Soc.* **2001**, 123(28), 6840-6846.

48. Strable, E.; Bulte, J. W. M.; Moskowitz, B.; Vivekanandan, K.; Allen, M.; Douglas, T. *Chem. Mater.* **2001**, 13(6), 2201-2209.

49. Atkins, P. and Shriver, D. *Inorganic Chemistry*. New York: W. H. Freeman and Co. 1999.

50. van Heerbeek, R.; Kamer, P. c. J.; van Leeuwen, P. W. N. M.; Reek, R. N. H. Dendrimers as Support for Recoverable Catalysts and Reagents. *Chem. Rev.* **2002**, 102(10), 3717-3756.

51. Bhyrappa, P.; Young, J. K.; Moore, J. S.; Suslick, K. S. *J. Am. Chem. Soc.* **1996**, 118(24), 5708-5711.

52. Reetz, M. T.; Lohmer, G.; Schwickardi, R. *Angew. Chem. Int. Ed. Engl.* **1997**, 13/14, 1526-1527.

Appendices

Appendix 1: ^{1}H NMR Spectral Overlays for Chapter 2.

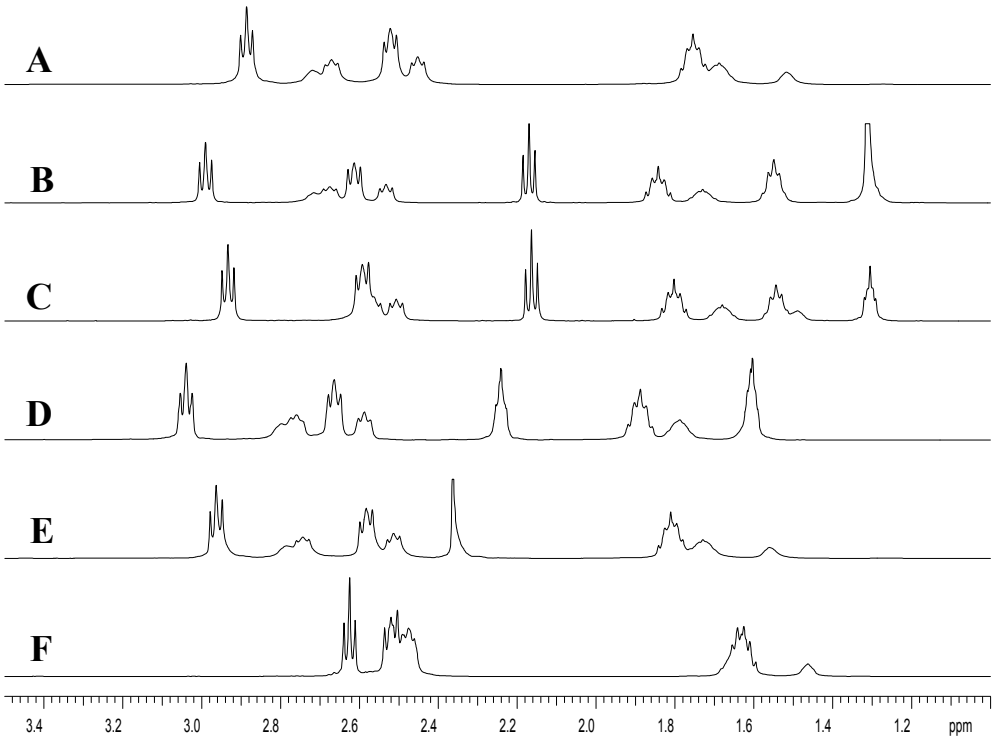

Figure A1.1. Stacked plots of ^{1}H NMR spectra of PPI-2 self-assembled with (A) phthalic acid; (B) sebacic acid; (C) suberic acid; (D) adipic acid; (E) succinic acid; (F) alone.

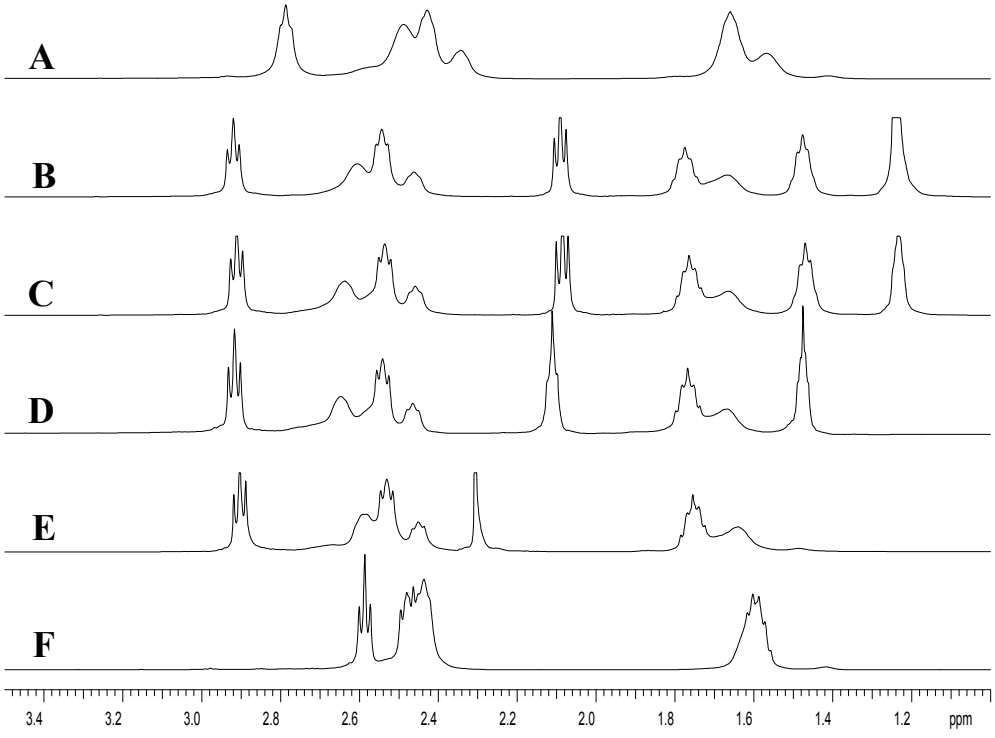

Figure A1.2. Stacked plots of ^{1}H NMR spectra of PPI-4 self-assembled with (A) phthalic acid; (B) sebacic acid; (C) suberic acid; (D) adipic acid; (E) succinic acid; (F) alone.

Appendix 2: 2D ^{1}H-^{13}C HETCOR Spectra for Chapter 2.

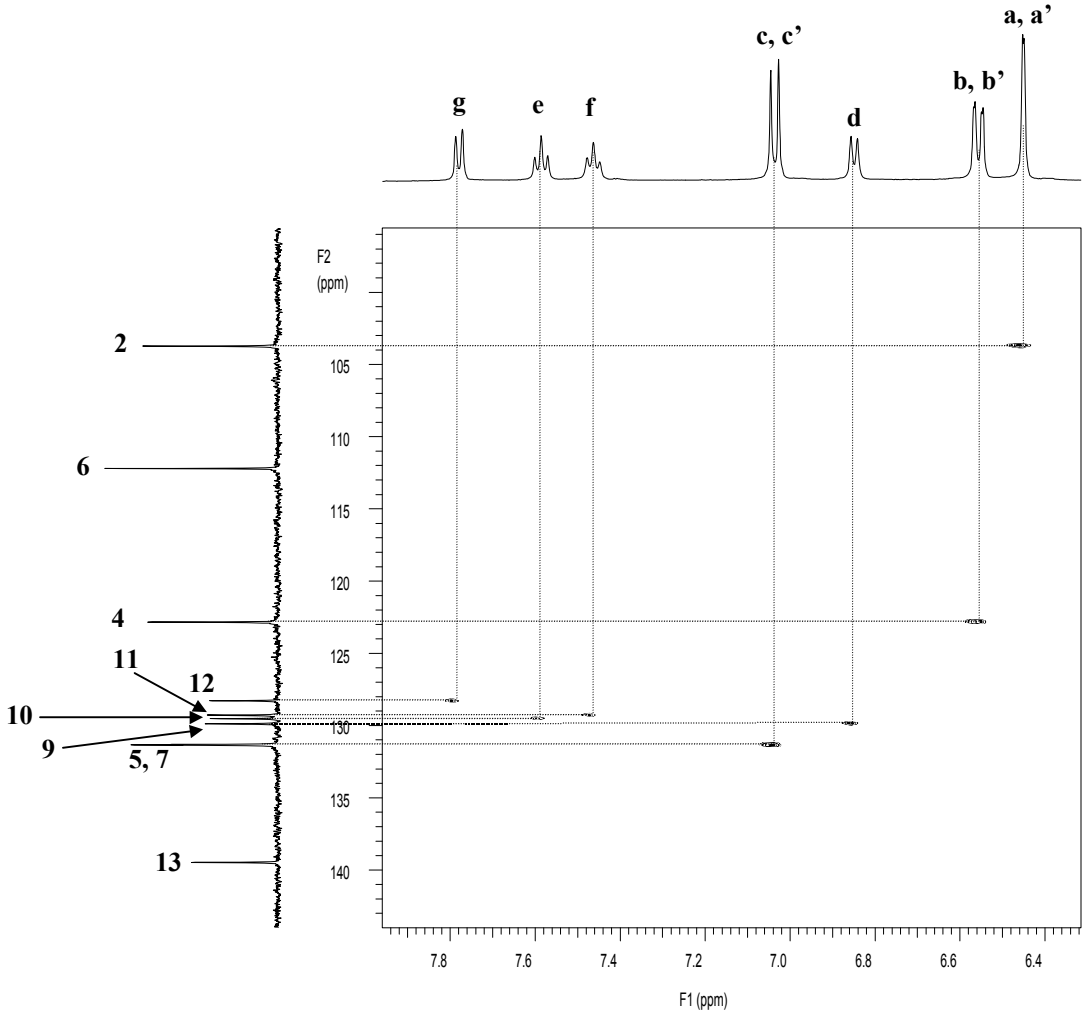

Figure A2.1. 2D ^{1}H-^{13}C HETCOR spectrum of fluorescein alone in D_2O.

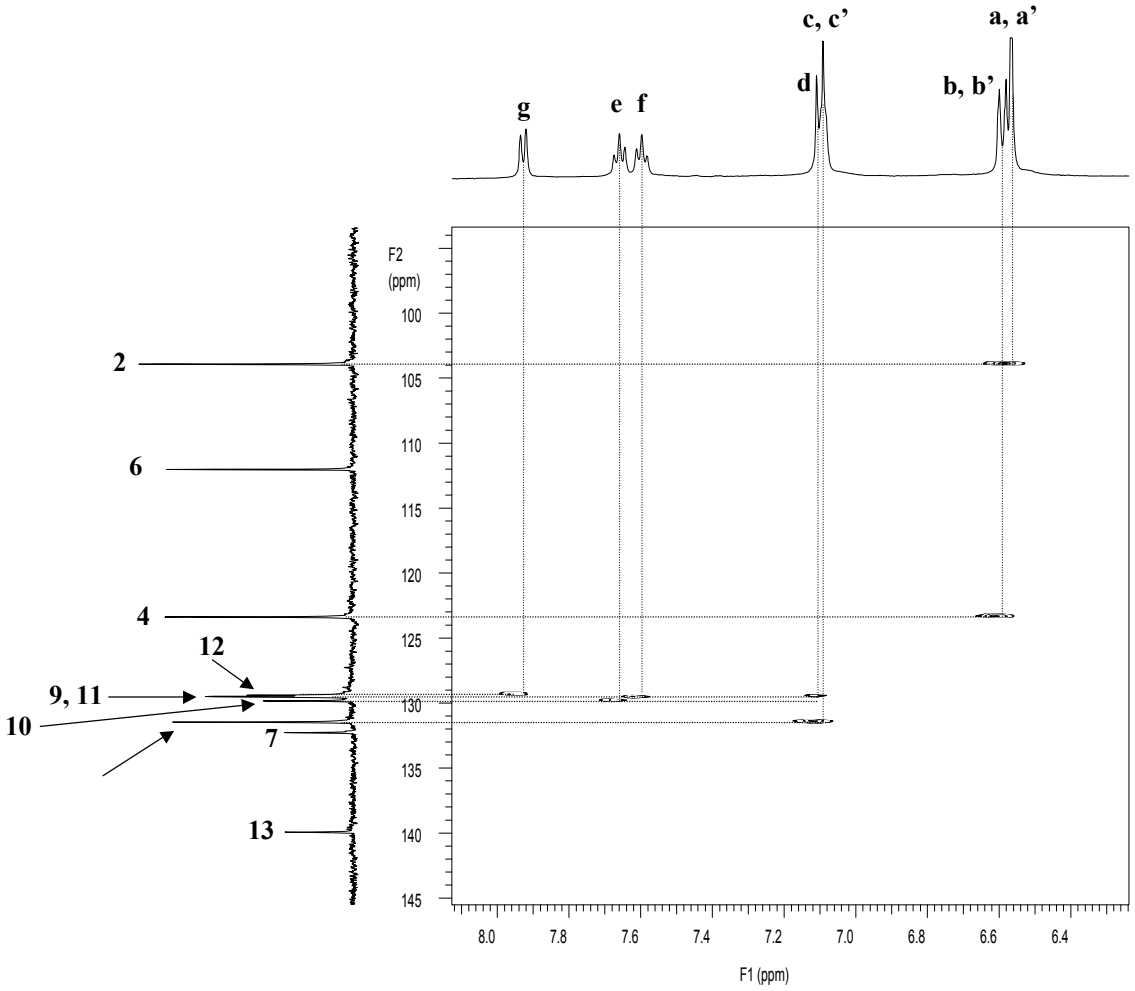

Figure A2.2. 2D ^{1}H-^{13}C HETCOR spectrum of fluorescein with PPI-3 in D_2O.

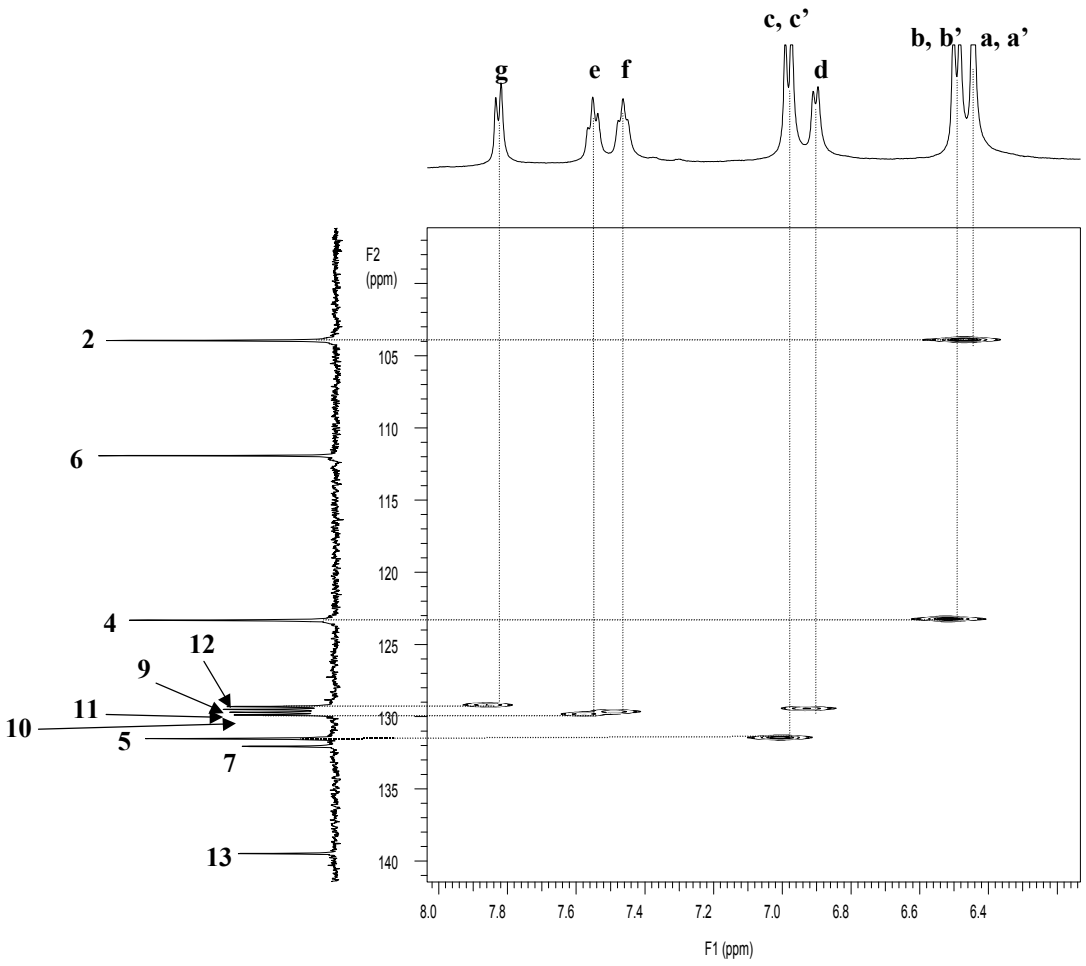

Figure A2.3. 2D ^{1}H-^{13}C HETCOR spectrum of fluorescein with PPI-3/adipic acid self assembly in D_2O.

Appendix 3. UV-vis Spectra and Analysis for Cu(II)/Co(II)/PPI-3 and Cu(II)/Zn(II)/PPI-3 Mixtures.

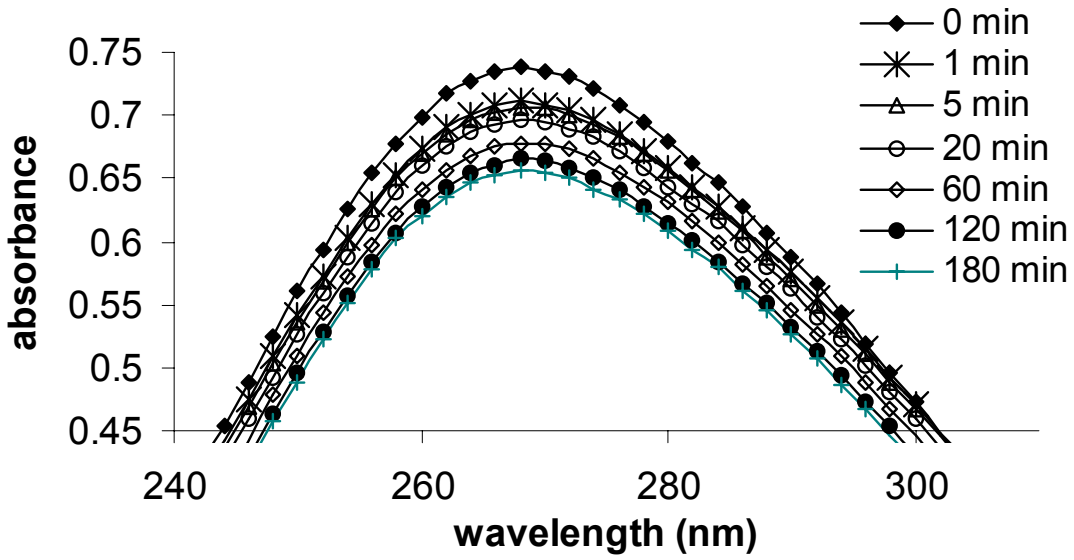

Figure A3.1. UV-vis spectra of Cu(II)/Co(II) mixture with PPI=3 at different times in H_2O.

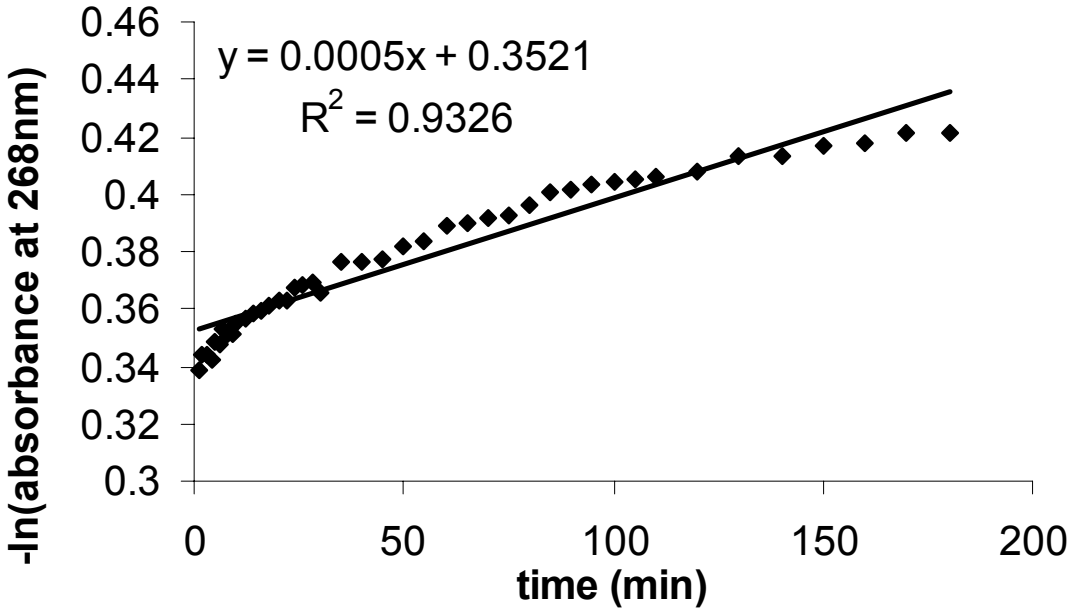

Figure A3.2. Plot of $-\ln(\text{absorbance}_{268nm})$ verses time for Cu(II)/Co(II)/PPI-3 mixture in H_2O.

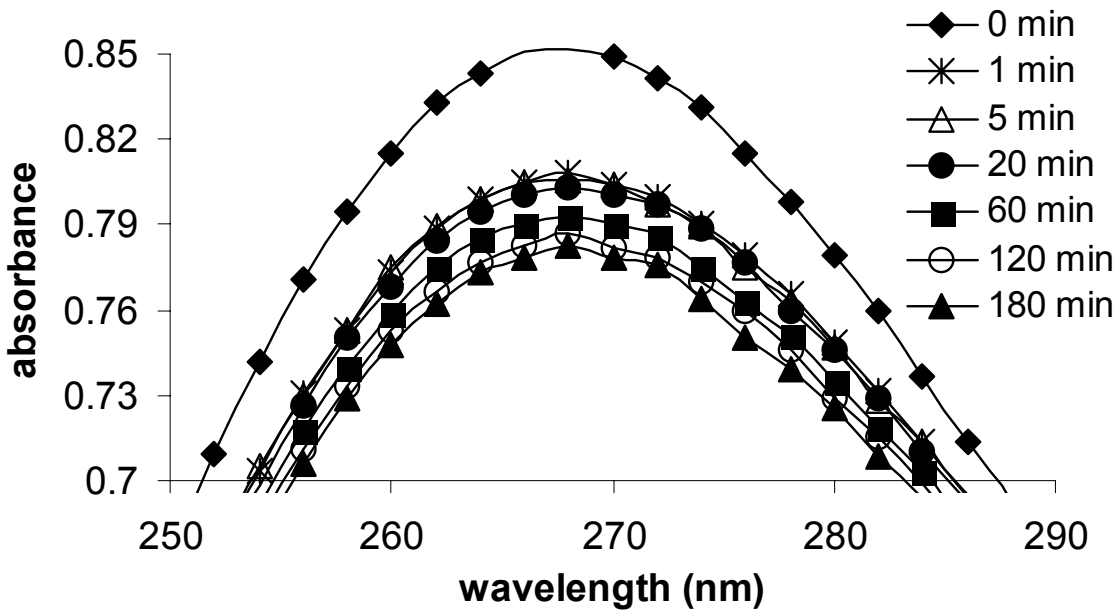

Figure A3.3. UV-vis spectra of Cu(II)/Zn(II) mixture with PPI=3 at different times in H_2O.

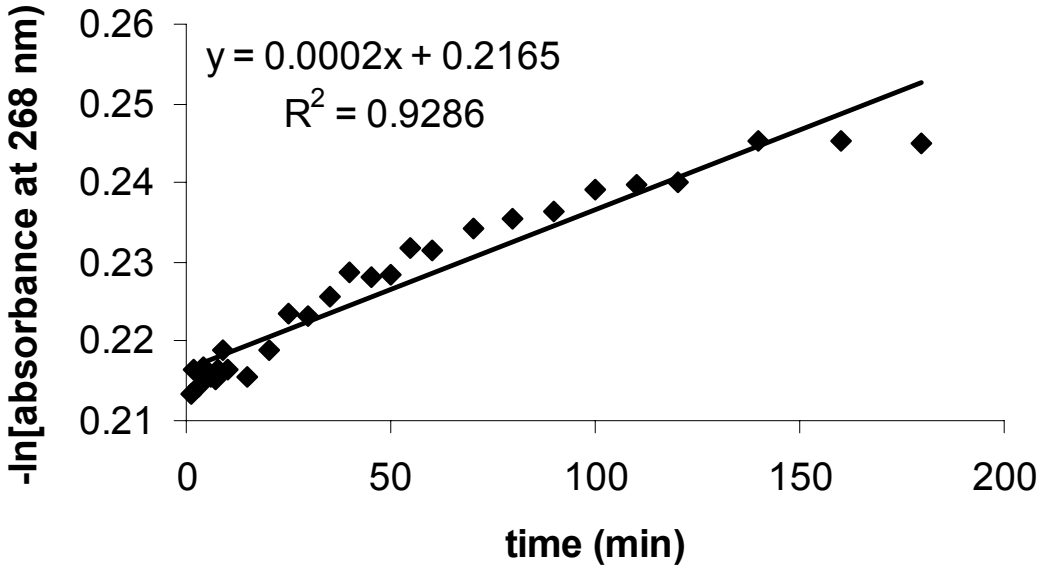

Figure A3.4. Plot of $-\ln(\text{absorbance}_{268nm})$ verses time for Cu(II)/Zn(II)/PPI-3 mixture in H_2O.